**Benha University**
**Faculty of Engineering Shoubra**
**Engineering Mathematics and**
**Physics Department**

# Fragmentation Characteristics of 3.7A GeV $^{16}O$ Interacting with Emulsion Nuclei

Thesis
Submitted to
Benha University - Faculty of Engineering Shoubra
In Partial Fulfillment of the Requirements for the Degree of
Doctor of Philosophy

In
Engineering Physics
By
Engineer

**Abdelnasser Saber Abdelfatah Soliman**

Assistant Lecturer in Engineering Mathematics and Physics Department
Faculty of Engineering Shoubra, Benha University

Supervisor

**Prof. Dr. A. Abdelsalam**

Professor of Nuclear Physics
Physics Dept.
Faculty of Science
Cairo University

**Prof. Dr. M. S. El-Nagdy**

Professor of Nuclear Physics
Physics Dept.
Faculty of Science
Helwan University

**Prof. Dr. B. M. Badawy**

Professor of Nuclear Physics
Reactor Physics Dept.
Nuclear Research Center
Atomic Energy Authority

**Dr. A. M. Abdalla**

Assist. Professor of Eng. Physics
Eng. Mathematics and Physics Dept.
Faculty of Engineering - Shoubra
Benha University

2017

وعلمك ما لم تكن تعلم وكان

فضل الله عليك عظيماً

صدق الله العظيم

(سورة النساء الآية ١١٣)

*To*

*My Father*

*(God rest his soul)*

*My Mother*

*And*

*My Wife*

## *Forward*

*This work was carried out at Mohamed El-Nadi, High Energy Laboratory, Physics Department, Faculty of Science, Cairo University, Egypt.*

# *Acknowledgment*

*First of all I* am *deeply thankful to* ***Allah*** *the most merciful and most graceful who without* ***Allah*** *help my efforts have gone astray. I wish to express my sincere gratitude and deepest appreciations to my supervisors.*

*I'm extremely grateful to* ***Prof. Dr. A. Abdelsalam****, Professor of Nuclear Physics, Faculty of Science, Cairo University, for suggesting the point of research, his continuous guidance, valuable discussion and scientific supervision that enabled me to accomplish this study.*

*Particular gratitude and deeply thanks to* ***Prof. Dr.*** **M. S. El-Nagdy,** *Professor of Nuclear Physics, Faculty of Science, Helwan University, for valuable guidance, support and continuous encouragement through the progress of this work.*

*My great thanks for* ***Prof. Dr. B. M. Badawy,*** *Professor of Nuclear Physics, Atomic Energy Authority, for his own great efforts in computer programs, continuous constructive discussion, advice and valuable revision during the progress of this thesis.*

*It is a great pressure to express my deep appreciation to* ***Assist. Prof. Dr. A. M. Abdalla,*** *Department of Engineering Mathematics and Physics, Faculty of Engineering Shoubra, Benha University, for providing many facilities during experimental work, helpful comments and his great efforts during my Ph.D. research.*

*My deepest gratitude to* ***Prof. Dr. O. Osman,*** *Professor of Nuclear Physics, Faculty of Science, Cairo University for his own great efforts and valuable revision for this thesis.*

Acknowledgment

*Most heartfelt thanks are to* ***Dr. Hytham A. A.,*** *for his continuous guidance, precious advices and continuous support.*

*I would like to thank all the current and former staff members of Mohammed El-Nadi High Energy Laboratory, Physics Department, Faculty of Science, Cairo University, Giza, Egypt.*

*It is pleasure to thank Prof. P. I. Zarubin at high energy laboratory at JINR, Dubna, Russia, for providing us the irradiated plates.*

*Also, I would like to express my sincere gratitude to Staff members of Engineering Mathmatics and Physics department-Faculty of Engineering Shoubra for providing many facilities, continuous encouragement and support that enabled me to complete this work.*

*Finally, I would like to express my endless thanks to most loving family members, relatives and friends for all their love and encouragement*

*Abdelnasser Saber*

# Aim of the Work

This work aims to investigate some physical phenomena dealing with the structure of oxygen nucleus as well as its fragmentation characteristics. It can be carried out using 3.7A GeV $^{16}O$ interactions in nuclear emulsion compared with other energy at 60A GeV.

# Abstract

In this experimental work, the projectile fragmentation of 3.7A GeV $^{16}O$ interaction with emulsion nuclei is investigated.

Throughout a total scanned length of 195.58 meters, 1540 inelastic interactions are picked up. The measured mean free path is 12.70±0.33 cm, which corresponds to interaction cross-section = 988 ±25 mb. This value is compatible with those calculated on the basis of a geometrical consideration.

The delta-ray counting method is used to identify the charge of each of projectile fragment. The delta ray distribution of each charge is fitted by a Gaussian shape. The fragmentation topology of $^{16}O$ is presented and compared with that obtained in the interaction of $^{16}O$ with emulsion nuclei at 60A GeV. The results show that the mechanism responsible for projectile fragmentation is independent of the projectile energy.

The probabilities of the different produced projectile fragments indicate that the He is the most probable channel. This implies that $^{16}O$ structure tends to have clustering behavior. This clustering effect is independent of the incident beam energy.

The events associated with single nucleon participations are supposed to be due to a single charge particle or neutron stripped from the projectile. The multiplicity characteristics of particles produced from these events are compared with those due to p-Emulsion interaction at the same energy as well as the prediction of the cascade-evaporation model. The study shows that the interactions of these stripped nucleons occur only with a free or quasi free nucleon with the absence of cascading.

# Contents



## Chapter (1)

## Review of High Energy Nucleus-Nucleus Collisions

## Chapter (2)

## Experimental Techniques & Methods of Measurements



## Chapter (3): Results and Discussions

# List of Figures

# List of Tables

**The symbols and abbreviations used in this thesis are given below:**

| Physical quantity | Symbol |
|---|---|
| The energy density of normal nucleus. | $\varepsilon_0$ |
| Joint Institute of Nuclear Research. | **JINR** |
| Super Proton Synchrotron. | **SPS** |
| European Center for Nuclear Research. | **CERN** |
| Alternating Gradient Synchrotron. | **AGS** |
| Brookhaven National Laboratory. | **BNL** |
| Lawrence National Berkeley Laboratory. | **LBNL** |
| Quark gluon plasma. | **QGP** |
| Shrinkage factor of the emulsion. | **K** |
| Grain density of the track. | **g** |
| Minimum value of the grain density. | $g_0$ |
| Normalized grain density. | $g^*$ |
| Cone emission angle. | $\theta_c$ |
| Velocity of secondary particles. | $\beta = v/c$ |
| Charge number. | **Z** |
| Mass number. | **A** |
| Projectile mass number. | $A_P$ |
| Target mass number. | $A_T$ |
| Mass number of the $i^{th}$ emulsion nucleus. | $A_i$ |
| The Impact parameter. | **b** |

| | |
|---|---|
| Radius of the projectile nucleus. | $\mathbf{R_P}$ |
| Target nucleus Radius. | $\mathbf{R_T}$ |
| The effective collision radius. | $\mathbf{r_{eff}}$ |
| Concentration of the $i^{th}$ emulsion nucleus per $Cm^3$. | $\mathbf{N_i}$ |
| Inelastic Reaction cross section of the projectile with the $i^{th}$ type of the emulsion nuclei. | $(\sigma_i)$ |
| Total Inelastic reaction cross Section. | $(\sigma_{Inel.})$ |
| Experimental values of interaction mean Free paths. | $(\lambda_{exp.})$ |
| Theoretical values of interaction mean Free Path according to different models. | $(\lambda_{Cal.})$ |
| Longitudinal momentum per nucleon of the incident projectile. | $\mathbf{P_{beam}}$ |
| Average transverse Fermi momentum per nucleon in the incident nucleus. | $\mathbf{P_{Fermi}}$ |
| The number of delta ray produced. | $N_\delta$ |
| Projectile fragments in the emission cone within angle of $\theta_c \leq 3^o$. | **PFs** |
| Charge of Projectile fragment. | $\mathbf{Z_{PFs}}$ |
| Number of doubly charged Projectile fragments (alpha). | $\mathbf{N_{alpha}}$ |
| Number of singly charged Projectile fragments. | $\mathbf{N_p}$ |
| Number of multiply charged Projectile fragments. | $\mathbf{N_F}$ |
| The summation of the charges of projectile fragments in the emission cone within angle of $3^o$. ($\mathbf{Q} = \sum \mathbf{Z_{PFs}}$ ). | **Q** |

| | |
|---|---|
| The Shower Particles Multiplicity. | $\mathbf{N_s}$ |
| The Average Value of the Shower particles Multiplicity. | $\langle N_s \rangle$ |
| The Grey particles Multiplicity. | $\mathbf{N_g}$ |
| The Average Value of the Grey particles Multiplicity. | $(< \mathbf{N_g} >)$ |
| The Normalized Multiplicity Distributions of the Grey particles. | $(\mathbf{P(N_g)})$ |
| The Black particles Multiplicity. | $(\mathbf{N_b})$ |
| The Average Value of the Black particles Multiplicity. | $(< \mathbf{N_b} >)$ |
| The Normalized Multiplicity Distributions of the Black particles. | $(\mathbf{P(N_b)})$ |
| The Heavily ionizing particles multiplicity. | $(\mathbf{N_h})$ |
| Nucleon-Nucleon interaction | **N-N** |

# Preface

An extensive amount of experimental data on high energy nuclear collisions provided great aspects in nuclear physics and reaction mechanisms. In Lawrence Berkeley National Laboratory (LBNL) efforts were directed to describe nuclear fragmentation experimentally and theoretically [1-5]. So far, this subject has been of interest [6].Observations of the fragmentation of light relativistic nuclei open up new opportunities to explore highly excited near multiparticle decay threshold [7].Such states has a loosely bound systems with spatial spread significantly exceeding the fragment sizes. The objective of the present thesis is devoted to progress the study of the projectile fragmentation of $^{16}O$ nuclei at the energy of 3.7A GeV in nuclear emulsion from Dubna. The projectile fragmentation at high energy is believed to be more efficient in the following:

I. Improving our understanding of the various mechanisms that contribute to the continuum projectile spectra.
II. Reflecting the internal structure of the projectile, namely the cluster structure and distribution of the break-up products (fragments) of the projectile.

The present thesis is classified into three chapters. Chapter 1 contains a review of high energy nucleus-nucleus collisions.

Chapter 2 presents the experimental technique used in the terminology of emulsion experiment as well as the criteria used to identify the projectile fragments. Chapter 3 is devoted to analyze and discuss the experimental results. Finally, the observed conclusions are drawn.

## 1.1 Introduction

One of the particular interests at high energy nucleus-nucleus collisions is to study the fine properties of nuclear matter. It allows a creation of medium with high density to undergo a phase transition into quark gluon plasma (QGP) at temperature ~200 MeV or energy densities ~ (2-3)$\varepsilon_o$ [8], where $\varepsilon_o$ is the energy density of normal nucleus.

Since 2000, a first milestone in the search for QGP was the CERN press announcement. The Pursuit of the extreme state of matter has been the focus of many experiments in the program of Brook National Laboratory (BNL). In 2005, the creation of an extreme state of matter had been announced by the four major RHIC experiments (PHENIX, STAR, PHOBOS and BRAHMS) of BNL [9].The discovery of a hot and dense state matter bears many properties of the predicted QGP.

Recently, the study of ultra-relativistic collisions in the center mass system has become a subject of great interest. At LHC in CERN, several experiments had been processed by ALICE [9], CMS [10] and ATLAS [11] with the hope that they will lead to a novel domain of nuclear matter consisting of high density and temperature which may have been reached in the hot early universe.

## 1.2 Energy domains of heavy ion physics

Heavy ion collisions can be classified according to the collision energy into three main regions:

**1-Intermediate heavy ion reactions**

The corresponding beam energies are in the range 10A-100A MeV.

In this region the properties of hot nuclear matter can be studied around the normal nuclear density (the atomic nucleus density, averaging about $2.3\times10^{17}$ Kg/m$^3$). The accelerators doing research in this energy domain are, for example,

the NSCL at Michigan state University, UNILAC and SIS at GSI in Darmstadt Germany.

**2- Relativistic heavy ion reactions**

The corresponding beam energies are in the range 0.1A-10A GeV. In this region the compressibility and other basic properties of nuclear interactions, such as, phase transition can be tasted. This is the area where the research is mostly developed. Moreover, real quantitative questions on nuclear compressibility, medium cross section, momentum dependence of nucleon-nucleon interaction, etc., are studied. This energy range is studied at some accelerators like the Synchrophasotron of JINR in Dubna, Bevalac at LBNL and SATURN in Saclay France.

**3- Ulra-relativistic heavy ion reactions**

This region starts at about 10A GeV and concerns mainly with quark-gluon plasma search. This energy range has been provided by some accelerators as SPS at CERN and the AGS at Brookhaven National Laboratory (BNL).

## 1.3 Classification of nuclear collisions

Theoretically the collision geometry is determined by the impact parameter, b, defined as the distance between the straight line trajectories of centers of the two nuclei before their interaction as shown in Fig. (1-1a) and Fig. (1-1b).The impact parameter is not directly measurable. In high energy nucleus-nucleus collisions there are various modes of interaction:

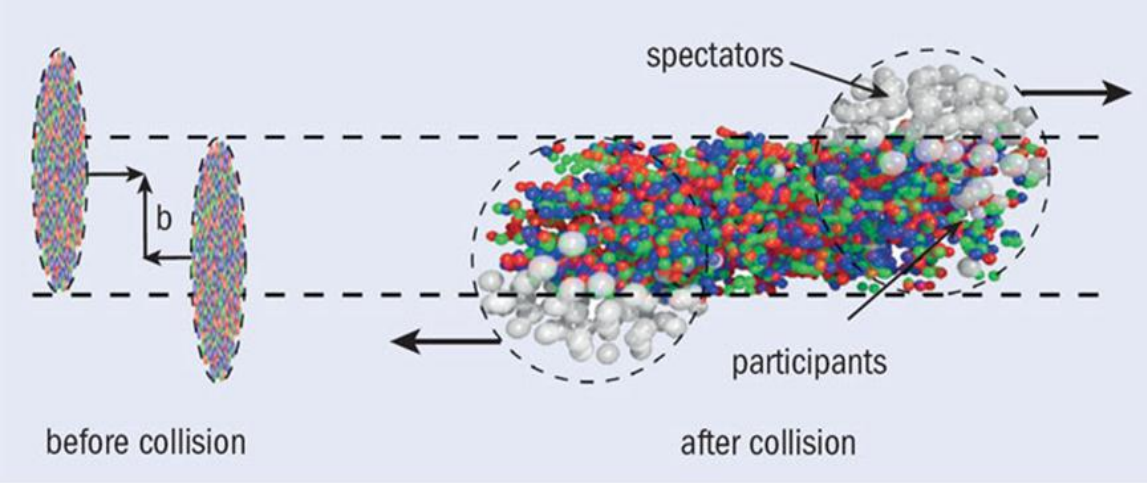


**Fig. (1-1a):** Schematic presentation of the impact parameter.

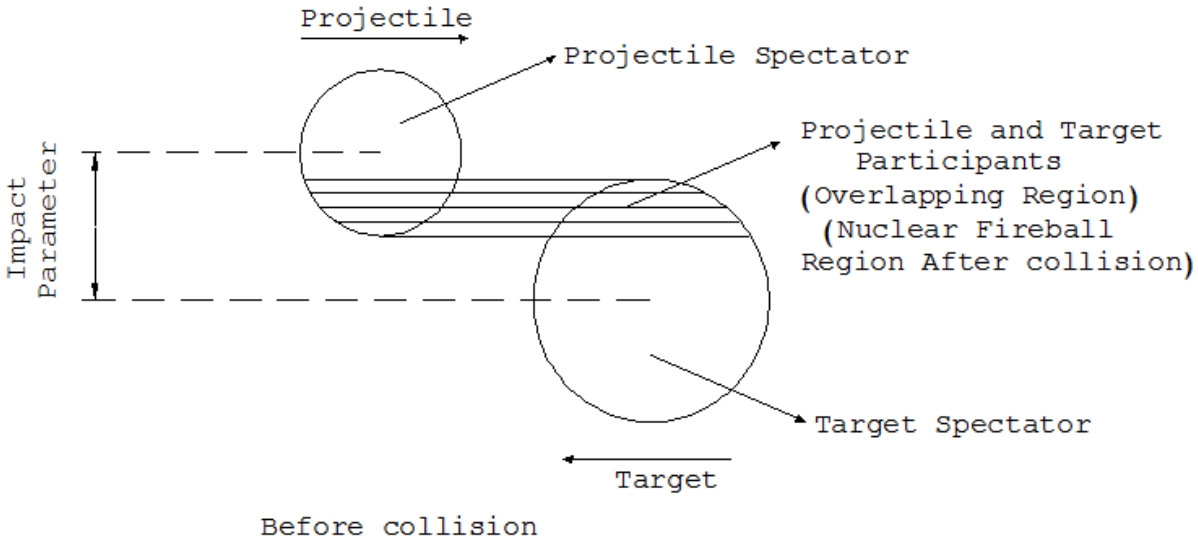


**Fig. (1-1b):** Schematic diagram of the fragmentation system of target and projectile in nucleus–nucleus collisions.

## 1 .3.1 Electromagnetic dissociation

The electromagnetic dissociation occurs when the value of impact parameter is larger than the range of nuclear force [12] as shown in Fig. (1-2), so that no nuclear interactions occur; extremely strong electromagnetic fields are produced for a short time at the nucleus [13].This process is called the electromagnetic dissociation (EMD) [14, 15]. In this case, a virtual photon is exchanged between a target nucleus and projectile. In case of projectile dissociation process, the

projectile nucleus is excited by the virtual photon absorption from electromagnetic field of the target nucleus and then decays by particle emission [15-17]. In this case there are two main characteristics:

1-The interaction shows no sign of target fragmentation (white star).

2- The fragmentation cone is defined by $\theta$ given by $\langle Sin\theta \rangle = \frac{P_{Fermi}}{P_{beam}}$ where $P_{Fermi}$ is the average transverse Fermi momentum per nucleon in the incident nucleus (~200 MeV/c) and $P_{beam}$ is the longitudinal momentum per nucleon of the incident projectile(4.5 GeV/c). Consequently, the value of $\theta$ at incident energy of 3.7A GeV is calculated to be 44 mrad ($\approx 3^{o}$).

On the other hand, the target dissociation process is possible if the target nucleus absorbs the virtual photon from the electromagnetic field of the projectile and then decays [18].

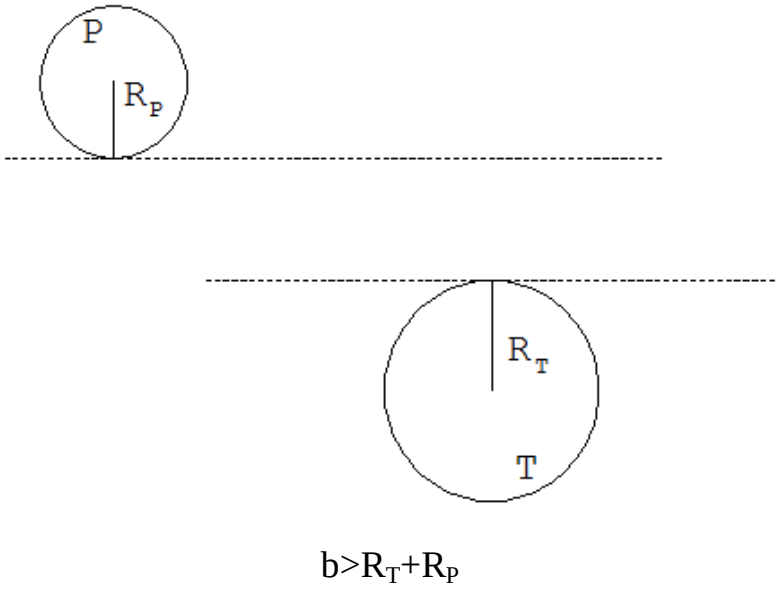


**Fig.(1-2):** Schematic diagram of electromagnetic dissociation.

### 1.3.2 Peripheral collisions

Fig. (1-3) shows the schematic diagram of the peripheral collisions. In peripheral collisions, when the impact parameter "b" is given in the form

$$b \approx R_T + R_P$$

where, $R_P$ and $R_T$ are the radii of the projectile and target nuclei, respectively, only a small momentum is transferred between the nuclei. So, in these reactions, one or both of the nuclei disintegrate through a fragmentation process. The projectile fragments (PFs) resulting from peripheral collisions are emitted in a narrow forward cone whose angular width can be determined by the intrinsic Fermi-momentum distribution of the nucleons within the fragmented projectile nucleus [19, 20]. Target fragmentation is also produced in this collision where the angular distribution of such fragments is anisotropic.

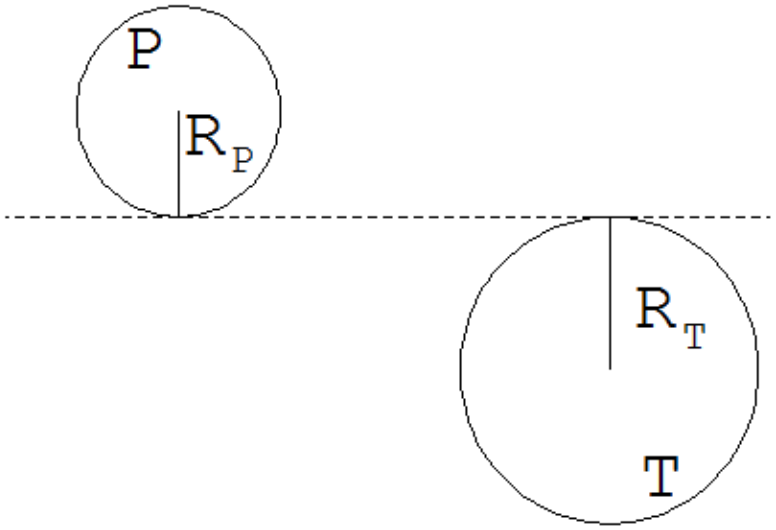


$$b \approx R_T + R_P$$

**Fig.(1-3):** Schematic diagram for peripheral interaction.

### 1.3.3 Quasi–central collisions

If the value of the impact parameter of the collision between two nuclei ranges from the difference to the summation of the radii of these nuclei as given in the form

$$|R_T - R_P| < b < R_T + R_P$$

A partial overlap takes place between the projectile and target nuclei**,** so some nucleons from both the projectile and target participate in the collision [19, 20]. Fig. (1-4) shows the schematic diagram of the quasi-central reaction.

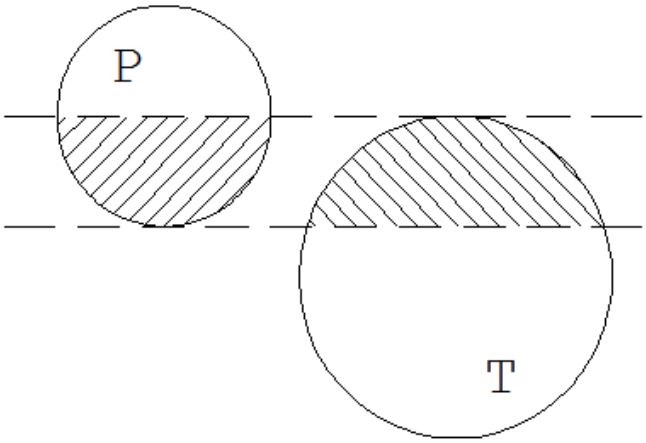


$$|R_T - R_P| < b < R_T + R_P$$

**Fig.(1-4):** Schematic diagram for Quasi central interaction.

### 1.3.4 Central collisions

In these collisions, the impact parameter can carry values from 0 to $|R_T - R_P|$. When b = 0, it is called head-on collision, where a complete overlapping between the projectile and target nuclear matter takes place, i.e. the two nuclei penetrate through each other. When collisions having $0 \le b \le |R_T - R_P|$ are allowed, it is called minimum-bias collision. The schematic diagram of the central

collision is shown in Fig. (1-5). In this type of collisions there is no projectile fragments produced. These violent reactions produce a large number of secondaries distributed mostly over the forward hemisphere [21]. So the large multiplicity of particles beside the absence of projectile fragmentation acts as signatures for a central collision.

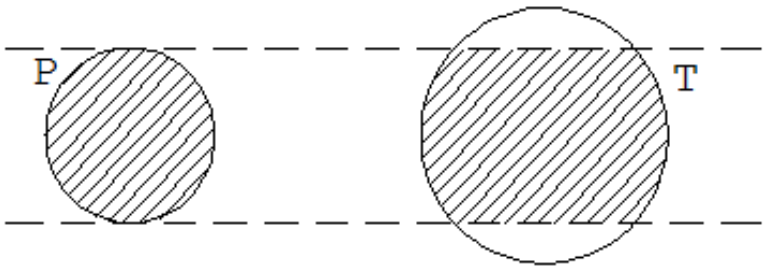


$$0 \leq b \leq \left| R_T - R_P \right|$$

**Fig. (1-5):** Schematic diagram for central interaction.

## 1.4 Mean free path and inelastic interaction cross section

The reaction probability is usually expressed in terms of nuclear reaction cross section $\sigma_R$ which is the effective area possessed by a nucleus for removing the incident particles from a collimated beam.

Glauber's multiple scattering theory [22, 23] has been used to predict nucleon–nucleus total cross–sections accurately in the few GeV range. The formalism involves the folding of the basic nucleon–nucleon scattering amplitudes with known nuclear matter distribution. The theory has been extended to nucleus-nucleus collisions [24] and used to predict the total inelastic cross-sections. The theory is essentially geometrical and the following proportionality is predicted from it,

$$\sigma_{\text{inel.}} \propto (A_T^{1/3} + A_P^{1/3})^2$$

The best parameterization is given by [25],

$$\sigma_i = \pi r_o^2 [A_P^{1/3} + A_T^{1/3} - \beta (A_P^{-1/3} + A_T^{-1/3})]^2 \qquad (1-1)$$

where $r_o = 1.32 \pm 0.01$fm and $\beta = 0.85 \pm 0.03$

There are several theoretical models [21, 26-36] have been introduced to study the nucleus-nucleus reaction cross section $\sigma_R$, from which are presented as the following:

### 1.4.1 Hard sphere model

The reaction cross section $\sigma_R$ according to the hard sphere model [26] is given by:

$$\sigma_i = \pi r_o^2 (A_P^{1/3} + A_T^{1/3})^2 \quad \text{fm}^2 \qquad (1-2)$$

where $r_o$ is constant of proportionality for the geometrical nuclear radius, $r_i = r_o A_i^{1/3}$ and $r_o = 1.48$ fm.

It was suggested by Bradt and Peters [26], that the effective collision radius "$r_{eff}$" is equal to the geometrical nuclear radius $r_i = r_o A_i^{1/3}$ minus a certain decrement $\Delta r$. Accordingly the collision cross section is:

$$\sigma_i = \pi (r + r_i - 2\Delta r)^2 \qquad (1-3)$$

where r and $r_i$ represent the geometrical radii of the projectile nucleus and target nucleus, respectively. The interaction mean free path $\lambda$ is:

$$\lambda = (\sum_i N_i \sigma_i)^{-1} \qquad (1-4)$$

where $N_i$ is the number of the $i^{th}$ target nucleus per $cm^3$ in the emulsion.

### 1.4.2 Overlap model

According to the Overlap Model [29, 31, 33] the interaction cross section $\sigma_R$ is determined by

$$\sigma_R = \pi r_o^2 (A_P^{1/3} + A_T^{1/3} - b)^2 \quad \text{fm}^2 \qquad (1-5)$$

This equation is a modification of the hard sphere model, where b refers to the overlap parameter. It can be seen that eq. (1-5) is uncomplicated.

According to Glauber multiple scattering theory [34-36], the total nucleus-nucleus reaction cross section that expressed by Bradt- Peters formula [26] was expressed by Barshay [32] as

$$\sigma_R = \pi r_o^2 [A_P^{1/3} + A_T^{1/3} - b_o ( A_P^{-1/3} + A_T^{-1/3} )]^2 \quad fm^2 \qquad (1\text{-}6)$$

Heckman et al. [37] measured the mean free paths for the interactions of $^4$He, $^{12}$C, $^{14}$N and $^{16}$O with emulsion nuclei and by using the Bradt-Peters geometrical approximations [26]. They found that the experimental results can be best fitted by applying the parameters $r_o$ and b, as coupled parameters, lie in ranges $1.15 \leq r_o \leq 1.45$ fm and $0 \leq b \leq 1.5$[26,37,38].

## 1.5 Projectile and target fragmentation at relativistic high energy

According to the participant–spectator model [39, 40] as shown in Fig.(1-1a) and Fig. (1-1b), the participant part is the overlapping region of the nuclear volume. It is the first stage of collision which is very rapid, very hot and having short life time. In this part a sudden compression occurs to nuclear matter which is adequate for quark–gluon plasma formation. Many quarks-antiquarks are created. By successive collisions multiple productions of new particles occur. So the system will expand again. Finally nucleons are emitted individually, in clusters or in a fragment form. The spectator region, on the other hand, is the remaining parts of the nuclei that don't participate in the disintegration process of the projectile and target nuclei. A fraction of the available energy is transferred to the spectator parts of colliding nuclei leaving those colliding remnants in an excited state then the de-excitation occurs. In the target spectator region, initially the nucleons are at rest. After collision, a small fraction of projectile energy transfers to the target nucleons by diffusion. Then the system suffers multiple elastic scattering until it reaches equilibrium. Then the system evaporates producing heavily ionizing fragments. The projectile spectator region has momentum per nucleon almost equals that of the parent nucleus. Hence the projectile fragments are emitted inside a narrow forward angular cone centered on the direction of incident beam.

## 1.6 Alpha clustering in the fragmentation processes

Progress achieved in the study with relativistic nucleus beams gives rise to new approaches in solving some topical problems of the nuclear structure. Among them is a search for collective degrees of freedom in which separate groups of nucleons behave like composing clusters. Such a peculiar feature, clustering in excited nuclei, is revealed especially clearly in light nuclei, in which the possible number of cluster configurations is rather small. The natural components of such a picture are few-nucleon systems having no proper nuclear excitations. First of all of these are α-particles, as well as pairing proton and neutron states, deuterons, tritons and $^{3}$He nuclei. Possibly, the study of the decays of stable and radioactive nuclei to cluster fragments might reveal some new particularities of their origin and their role in cosmic-ray nucleosynthesis [41].

The most advantageous way for studying clustering is the use of peripheral interactions of relativistic nuclei which occur at minimal mutual excitations of colliding nuclei caused by electromagnetic interactions. The conservation of the electric charge and mass number of a projectile is one of the requirements of this study. The reliable and complete observation of the multiparticle relativistic fragmentation processes is a motivation for using nuclear emulsion technique. Emulsions make a great possibility to establish the most feasible charge channels of such processes.

## 1.7 Models for multiparticle production in high energy collisions

Many theoretical models have been introduced to interpret the different experimental facts for the multiple productions in hadron–nucleus collisions. Some examples are discussed in the following:

### 1.7.1 Fireball model

The nuclear fireball was explained in a model by Westfall et al [42].This model uses the geometrical concepts of the abrasion model, [43] the free expansion of an ideal gas, and the extension to higher energies, the statistical thermodynamics of strong interaction by Hagedorn [44]. It is assumed that the projectile and target are spheres that make clean cylindrical cuts through each other, leaving a spectator piece of the target, also a spectator piece of the projectile. As the De Broglie wavelength of the nucleons is small in the ultra-relativistic collisions, the nucleons can be classified into two categories: the nucleons in the overlap region which are designated as participants, the nucleons outside this area which are called spectators. In the basic picture, the spectators leave the system without suffering interactions and the participants undergo binary nucleon-nucleon, NN, collisions. The participant nucleons which are swept out from the projectile and target form the fireball in the overlapping region after collision. A spectator piece of the target is left. If the impact parameter is sufficiently large, a spectator piece of the projectile is also left. The fireball model enables the predictions of nucleon multiplicities and with some modifications, also pions inclusive spectra and multiplicities. The pion and delta abundance, and thus the finally observed pion yield are controlled by the locally defined multinucleon properties like density, temperature, and chemical potential [45, 46]. If the temperature or the density of the fireball becomes larger than the critical values ( $T_{critical} \sim 200$ MeV) QGP is created. The fireball starts to expand and cool, after which the quarks in the plasma will be eventually constructed into a large number of hadrons. This process is called hadronization. Most of hadrons will decay finally into pions. The model does not give any

answer as to how the system evolves from the original pieces of cold nuclear matter to the heated fireball.

### 1.7.2 Cascade evaporation model (CEM)

The multiparticle production in hadron-nucleus collisions over energy range from several dozens of MeV up to several GeV , is analyzed on the basis of CEM model [47-50]. In this model of hadron-nucleus collisions, the final state is assumed to be formed instaneously, i.e. the created particles become physical entities inside the nucleus.

In this case, the incident hadron interacts successfully with a number of nucleons inside the target nucleus producing secondaries which in turn have sufficient energy to produce tertiaries and so on.The generalization of the model for nucleus-nucleus collisions is made by Barashenkov and Toneev[51] , in which it was shown that the nucleus-nucleus interactions can be explained by the prediction of cascading mechanism. In other words the model explains the experimental results on the distributions and averages of the different emitted secondaries multiplicity.

On the other hand, the CEM model disregards many important effects such as the production of mesonic and barionic resonances, the finite time of secondary particle formation, variations in the mean nuclear field and the coalescence of nucleons[52].The calculations of product particles and correlations between slow and fast particles are expected to be sensetive to these details.To clarify the key problems encountered in the description of these features in the forward and backward hemisphere, it may be convenient to use this simplified approach as a first approximation. The sample of generated events consists of 5000 of interactions for each projectile-target combination. In comparison with the experimental data, the same definitions and conditions are applied. It should be noted that the above model applies to the situation where binary scattering is important and is recognized as the best model applied for smaller projectiles interactions with heavy nuclei in the intermediate energy range 1-10A GeV[53].

### 1.7.3 Modified cascade evaporation model (MCEM)

CEM model is satifactory in agreement with data at low and intermediate energies (up to few GeV). At higher energies, the number of particles produced exceeds the number of the internuclear nucleons while the mass of the residual nuclei can be several times of the mass of the initial nucleus. In this case CEM model is expected to be in conflict with the experimental data. The modified cascade evaporation model MCEM [54] has been introduced to include the formation time in multipticle production process. The creation of a hadron is not instantaneously but takes a time, so it is called "formation time". The inelastic interaction of two nuclei can be arranged into four groups:

1. Group A, interactions of the nucleons of the projectile nucleus with those from the target nucleus,
2. Group B, interaction of the cascade particles with the nucleons of the target nucleus,
3. Group C, interaction of the cascade particles with the nucleons of the incident nucleus and
4. Group D, interaction of the cascade particles with each other, so called cascade-cascade interactions.

The main features of MCEM model are the following:

1- Process of cascading takes place both in the projectile and target nucleus.
2- Cascade stage of projectile is completed when all cascade paricles have left both nuclei or have been absorbed by them.
3- Cascade-cascade interactions are taken into account.
4- All the interactions are ordered in time.
5- The formation time of both interacting nucleons and produced mesons is included into the process of cascading inside both colliding nuclei.

## 1.8 Literature review

EL-Nadi et al. [55] studied the projectile fragmentation in $^{32}$S-Em at 3.7A GeV and $^{28}$Si-Em at 14.6A GeV. They concluded that the charge and multiplicity distributions of projectile fragments PFs are nearly energy independent where the limiting fragmentation hypothesis is valid. Wang Er-Qin et al. [56] studied the multiplicity distributions of PFs at 4.5A GeV/ c $^{12}$C, $^{16}$O and $^{28}$Si, as well as 4.1A GeV/c $^{22}$Ne interactions in nuclear emulsion. They concluded that doubly charged PFs ($N_{alpha}$) particles are emitted from heavier projectile nuclei due to one source or come from one cluster. EMU01 [57] collaboration studied the doubly charged PFs, $N_{alpha}$ in $^{16}$O-Em collisions at 200A GeV. They observed one temperature of $N_{alpha}$ PFs. Yan and Hai [58] studied the multiplicity distribution of singly charged PFs ($N_p$) in $^{84}$Kr-Em collisions at 1.7A GeV. The multiplicity correlations between $N_p$ and $N_{alpha}$ could be explained by participant-spectator model of nucleus-nucleus collisions [39]. They [58]studied also the multiplicity distribution of singly charged PFs $N_p$ in $^{84}$Kr-Em collisions at 1.7A GeV with different target groups. Adamovich et al.[59] studied the multiplicity distribution of doubly charged PFs ($N_{alpha}$) for Au-Au and Pb-Pb collisions at 11.6A GeV and 158A GeV . They showed that the multiplicity distributions of doubly charged PFs are similar in all cases indicating that limiting fragmentation is reached already at 12A GeV. Meng and Hai [60] studied the projectile fragmentation of $^{16}$O at 3.7A GeV with different target nuclei in nuclear emulsion. They concluded that the limiting fragmentation of the projectile is already achieved at Dubna energy (3.7A GeV). Fakhraddin and Rahim[61]studied the multiplicity distribution of projectile fragments, PFs in interactions of $^{4}$He, $^{12}$C, $^{16}$O, $^{22}$Ne and $^{28}$Si at 4.1-4.5A GeV/c with emulsion nuclei.They studied the dependence of singly charged PFs ($N_p$), doubly charged PFs($N_{alpha}$) and multiply charged PFs ($N_F$) on the size of different target groups (H, CNO and AgBr).They concluded that the multiplicity distribution of $N_p$, $N_{alpha}$ and $N_F$ depend on projectile mass number $A_p$. Singly

charged PFs $N_p$ increases slowly with the target size, while $N_{alpha}$ and $N_F$ decrease for the heavier target.

El-Nadi et al., [62]studied the $N_{alpha}$ fragmentation in $^{28}$Si-Em interactions at 14.6A GeV and 3.7A GeV $^{28}$Si-Em as well as $^{32}$S-Em at 200A GeV. Ying et al.[63] studied the production cross-section of $N_{alpha}$ emitted in 10.7A GeV $^{179}$Au-Em interactions. The results were compared with those obtained from different projectiles at high energies. Otterlund [64] studied the angular distribution of projectile fragments in $^{16}$O –Em interactions with different target groups at 200A GeV. He reported that the angular distributions of PFs are Gaussian shaped and the projectile fragmentation in the peripheral interactions is very similar to that at 2A GeV beam energy. Kumar et al., [65] studied the angular distribution and pseudo-rapidity distribution of $N_{alpha}$ fragments for $^{28}$Si-Em at 14.6A GeV. They demonstrated an energy independent behaviour of limiting fragmentation in the projectile fragmentation region.

## 2.1 Nuclear track emulsion

The nuclear emulsion is a very useful tool in experimental physics for investigating atomic and nuclear processes. A photographic emulsion consists of large number of small crystals of silver halide embedded in gelatin. When charged particles pass through the emulsion, some of the halide grains are modified, but their modifications are invisible and this effect is described as the latent image formation. On immersing the nuclear emulsion plate in a reducing bath, called the "developer", the latent images are turned into grains of silver which appear black within the transparent gelatin. So, the tracks of charged particles through the nuclear emulsion plate could be seen under the microscope as trails of developed black grains. A true three–dimensional image of the particle trajectory is obtained. After processing the nuclear emulsion, it occupies less volume than before and consequently its thickness decreases. For any quantitative measurements of track densities, ranges and angles, it is necessary to know the exact original thickness of the emulsion layer at the time of the exposure divided by its thickness at the time of scanning. This ratio is called "the shrinkage factor (k)". This factor may be different at different depths in emulsion. Also it may vary from place to place in a given plate. The nuclear emulsion has many advantages that make it a very useful tool than other types of detectors. Some of these advantages are summarized in the following:

**1)** The emulsion can be used as a target as well as a detector of $4\pi$–space geometry.

**2)** It has the possibility of measuring energies and angles with high degree of resolution.

**3)** It can be used in studying the characteristics of new elementary particles and can detect the decay of the unstable neutral particles, rather than, its sensitivity to slow charged particles arising from the disintegration of the target nucleus.

**4)** Owing to the high stopping power of emulsion, a large fraction of short–lived particles are brought to rest in it before decay and hence their ranges and life times can be measured accurately.

According to the above mentioned advantages of the nuclear track emulsion, it seems that the nuclear emulsion is a suitable technique for studying the interactions of high energy particles with nuclei in which collisions occur with light nuclei like [carbon, nitrogen and oxygen] and heavy ones like [silver and bromine]. The less frequent interactions are the elementary collisions with the free hydrogen in the emulsion.

## 2.2 Details of the used emulsion stacks

In the present work, stacks of NIKFI-BR-2 nuclear emulsion type were exposed to 3.7A GeV $^{16}$O beam in Synchrophasotron at Dubna, Russia. Each emulsion pellicle of the stack has 600 μm thickness and $20\times10$ cm$^2$ dimensions. The chemical composition of NIKFI-BR-2 type is given in Table (2 –1). This table also gives the number of atoms per cm$^3$ corresponding to each element of the emulsion constituent

**Table (2-1):** Chemical composition of NIKFI-BR-2 emulsion.

| Element | Charge Number | Mass Number | Number of atoms/cm$^3$ $\times 10^{22}$ |
|---|---|---|---|
| H | 1 | 1 | 3.150 |
| C | 6 | 12 | 1.412 |
| N | 7 | 14 | 0.395 |
| O | 8 | 16 | 0.956 |
| Br | 35 | 80 | 1.028 |
| Ag | 47 | 108 | 1.028 |

## 2.3 Irradiation of the stack:

There are two types of the irradiation of the nuclear emulsion; the first type is the parallel irradiation in which the beam is parallel to the length of the stack, the second type is the perpendicular irradiation in which the beam is perpendicular to the X-Y plane of the stack, as shown in Fig. **(**2-1**)**. The type used in the present work is the parallel irradiation.

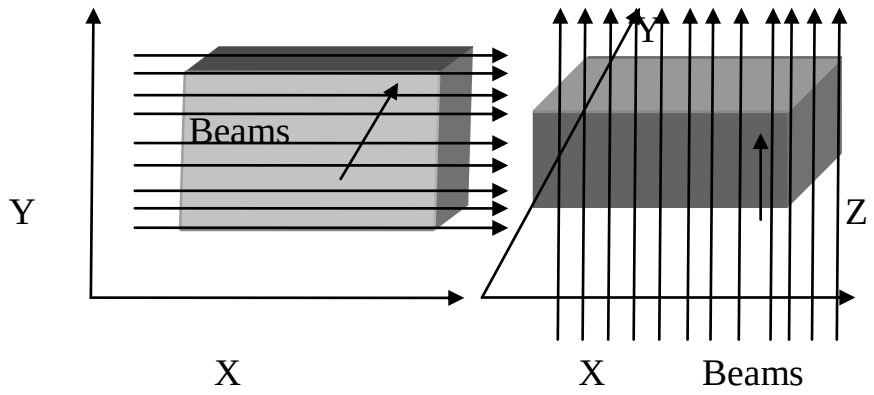


**Fig. (2-1):** Parallel Irradiation and Perpendicular Irradiation.

## 2.4 Microscopic description

In the present investigation two types of microscopes are used, one in the scanning and the other in the measuring respectively:

### 2.4.1 Scanning microscope

The scanning of the emulsion pellicles is carried out using 850050 STEINDORFF German microscope. A clear image is shown in Fig. (2-2). It has a stage of 18×16 $cm^2$ with an opening 7×2.5 $cm^2$. Stage adjustment in the X-direction is possible over a total length 7.8 cm with reading accuracy of the order of 0.1 mm. Oil immersion objective lens with magnification 100X is used for scanning the emulsion plates. Each primary track is picked up at the penetrating edge of the pellicles.

**Fig. (2-2):** Photographic picture of 850050 STEINDORFF German microscope.

### 2.4.2 Measuring microscope

In the present experiment, the Russian microscope (MSU–9) is used for measurements. It contains a rotatable metal stage 20×20 $cm^2$, which can rotate $360^o$ about the optical axis of the microscope. The motion of this stage in the X-direction can be allowed continuously or in adjustable fixed steps (cell length) of

100, 200 or 500μm. The motion in the Y-direction can be estimated using a measuring scale attached to one of the binocular eyepieces. This scale can be easily calibrated such that each division is corresponding to 16.6 μm with an accuracy of about 0.1 μm for the measurements in both X and Y directions. The motion in Z- direction which is read on a drum of one scale division of 1μm, through estimates up to 0.5 μm can be easily made. The Russian microscope contains a rotatable geniometer, of 360º measuring range with a reading accuracy of 0.1º.

The objective lenses used are:

1. 15X Binocular eyepiece.
2. Dry lenses with 10X and 40X magnification.
3. Oil immersion lenses with 60X and 90X magnification.

**Fig. (2-3):** Photographic picture of Russian Microscope (MSU-9).

## 2.5 Scanning techniques

There are two possible ways for scanning techniques are performed.

**1)** The area scanning.
**2)** The along-the-track scanning.

### 2.5.1 Area scanning

The area scanning of the pellicle is usually used for the search of events located in the nuclear emulsion volume; this is done by scanning field of view followed by field of view in strip position. For high efficiency, the field of view must be divided into a number of sufficiently small separated areas which are scanned throughout their depth. This method of scanning is useful in the cosmic ray studies, where the primary particles enter over a wide range of solid angles, in the case of neutral particles decay or when searching for certain type of interactions.

### 2.5.2 Along-the-track scanning

This way of scanning is the most useful technique used to locate all different kinds of events when the trajectories of the incident particles are almost in the plane of the nuclear emulsion. In this method, every track of the incident particles is followed along its length; until it interacts or leaves the pellicle. The location of each interaction of the incident projectile nuclei in the nuclear emulsion plates is registered in the scanning scheme with the aid of special squares on each plate (each square characterized by four numbers). In the present work, the along the track scanning is performed twice, where it is fast in the forward direction and slow in the backward direction; to be sure that the recorded events don't include interactions from the secondary tracks of the other interactions. Consequently, the scanning efficiency of picking up the events is nearly 100%.

## 2.6 Grain density and the specific ionization [66-67]

When charged particle passes through the photographic nuclear emulsion, it slows down via losing its kinetic energy due to inelastic interactions with the emulsion nuclei along its path. The charged particle loses its kinetic energy via the ionization of the silver halide grain and also via multiple elastic and inelastic

scattering. This leads to trails of ionized silver halides along its path. The grain density is defined as the number of developed grains of silver halides per unit path length of the particle track. It is denoted by g. It depends on some factors such as the degree of the development of the nuclear emulsion, the velocity and the charge of the ionizing particle. In order to obtain high accurate results, it is important to determine the normalized grain density $g^*$

$$g^* = \frac{g}{g_o} \tag{2-1}$$

where g is the observed grain density per 100 μm for the emitted secondary particles and $g_o$ is the grain density per 100 μm of relativistic track of minimum ionization. For Singly charged particle or electron, both values of g and $g_o$ is counted in the same plateau region and at the same depth in the nuclear emulsion. The most suitable method to measure the grain density is to count their number in a certain length of the selected track. The specific ionization is defined as the probability that at the passage of the ionizing particle through silver halide grains they are developed. It depends on the energy dissipated in silver halide grains. Hence, the specific ionization is a function of the energy loss of the particle. Owing to the variation in the degree of development through the depth of the emulsion, the grain density of each track must be measured in sections of different depths. In the present work $g_o$ is 30 grains per 100μm, which is the average over different emulsion plates.

## 2.7 Classification of the secondary charged particles

The tracks of the secondary charged particles are classified into three types according to the normalized grain density $g^*$ [66-67] which is determined by eq. (2-1). Fig. (2-4) shows a photographic picture of an inelastic interaction between the projectile and the target (star) observed in a nuclear emulsion plate as viewed under microscope.

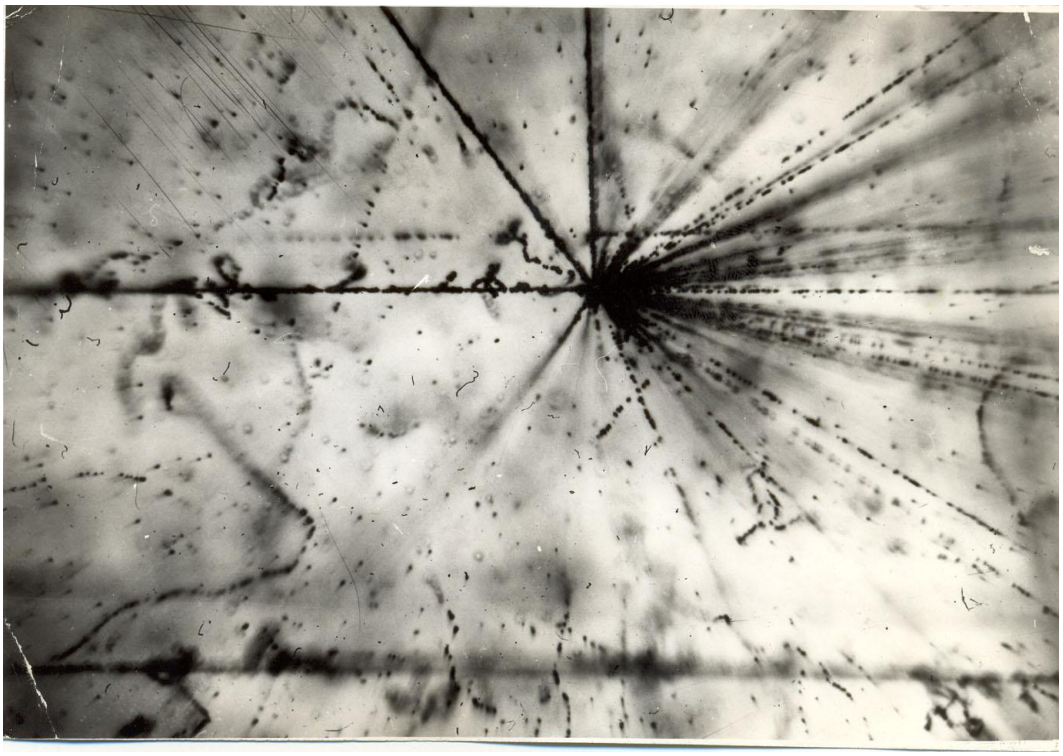

**Fig. (2-4):** Photographic picture of an inelastic interaction (star) observed in nuclear emulsion viewed under microscope.

### 2.7.1 Shower tracks

The shower tracks are due to the passage of the relativistic charged particles characterized by $g^* \leq 1.4$ and $\beta \geq 0.7$. Most of the shower particles are pions with energy (E > 70 MeV) contaminated with small fraction of fast protons with energy (E >400 MeV), charged K-mesons, antiprotons and hyperons. The shower particles multiplicity is denoted by $N_s$, which gives good estimates to the number of the charged π-mesons produced in the interaction.

### 2.7.2 Grey tracks

The grey tracks are due to the passage of slow particles characterized by the $1.4 < g^* < 10$, the value of the velocity $0.3 < \beta < 0.7$. Most of them are recoil target protons having range in the nuclear emulsion > 3000 μm, which correspond to proton energies 26 < E < 400 MeV. Some of the grey tracks may

be due to emitted deuterons, tritons, helium nuclei and nearly about 5% due to slow π-mesons. The grey tracks multiplicity is denoted by $N_g$.

### 2.7.3 Black tracks

The black tracks are characterized by the value of the normalized grain density $g^* \geq 10$, the value of the velocity $\beta \leq 0.3$. Most of them are evaporated target protons having range in nuclear emulsion ≤ 3000 μm, which correspond to energies E < 26 MeV. The black tracks may be also due to deuterons, α-particles and heavy fragments. The black tracks multiplicity is denoted by $N_b$. The grey tracks and the black tracks are known as tracks of the heavily ionizing particles. Their multiplicity is denoted by $N_h$.

$$N_h = N_g + N_b \qquad (2\text{-}2)$$

## 2.8 Identification of projectile fragments

The projectile fragments PF's are the spectator parts stripped from the incident nucleus during its interaction with the emulsion nuclei. They have an emission angle $\theta \leq 3^o$ in the forward direction. They are identified as:

1) Singly charged projectile fragments with Z = 1 (where Z is the charge) and $g^* < 1.4$
2) Doubly charged projectile fragments with Z = 2 and $g^* \approx 4$
3) Multiply charged projectile fragments with $Z \geq 3$ and $g^* > 6$.

The charge identification of singly charged projectile fragments is made by measuring the grain density g, which fulfills the criterion (1). For Z ≥ 2 fragments the delta-ray method is obeyed to identify the charge in this work.

### 2.8.1 Delta-ray counting method

When a charged particle passes through a material medium it interacts with some of its atomic electrons. The electrons which have enough energy to produce secondary ionization are knocked out. In sensitive nuclear emulsion these electrons produce short thin tracks emerging from the trajectory of the parent particles. These ejected electrons which have the ability to ionize other atoms are known as delta rays .The production of these rays depends on the charge and velocity of the parent particle.

For a projectile of charge Z and velocity of the parent particle β, the δ-ray density is given by [66]:

$$N_\delta = \text{Const.}\frac{Z^2}{\beta^2}\left[\frac{1}{W_{\min}} - \frac{1}{W_{\max}}\right] \qquad (2\text{-}3)$$

where β = v/c and $W_{min}$ is the minimum energy required to produce a visible δ-ray while $W_{max}$ is the maximum energy transferred to knock out electron. $W_{max}$ increases with β and consequently:

1) For non relativistic particles as β decreases the increase of both $1/\beta^2$ and $1/W_{max}$ terms is such that $N_\delta$ comes to a maximum value at a certain value of β.
2) At relativistic velocities where $\beta \to 1$, $1/W_{max}$ becomes small and consequently $N_\delta$ reaches a plateau value.

For velocities of the same order of magnitude, the maximum values of delta ray densities $N_{\delta 1}$ and $N_{\delta 2}$ produced by two particles of charges $Z_1$ and $Z_2$ respectively over residual ranges are connected by the relation:

$$\frac{N_{\delta 1}}{N_{\delta 2}} = \frac{Z_1^{\,2}}{Z_2^{\,2}} \qquad (2\text{-}4)$$

The complex appearance of δ-ray, however, makes it very difficult to establish a reliable set of counting criteria that ensures perfectly uniform and reproducible observations.

In this work, the measurements of projectile fragments are greatly simplified by the persistence of relativistic beam velocity. The ''grain '' criterion i.e. counting δ-ray with a different numbers of grains is employed and also δ-ray is counted over a track segment of 10 mm from the center of the interactions. These measurements are confined to a depth between 30 μm and 220 μm from the surface of the emulsion, and a distance of at least 3 mm from the edges. Under these conditions the corrections due to the variation of the degree of development of the plates can be neglected.

### 2.9 Systematic errors

Like other detectors, nuclear emulsion plates are not free from systematic errors. Systematic errors may be introduced in the emulsion plates due to:

1. The presence of background events that may result from the cosmic rays during the exposure time. These background events can be eliminated by choosing the incident beam track lies within $3^o$ with respect to the direction of incidence pellicle ( the real projectile beam has been selected).
2. Fading of tracks and the variation of the shrinkage factor with temperature which affect the measurements of the emission angles. To reduce the losses of track and minimizing the errors in the measurements of emission angles, events showing interactions within 20 μm from the top and the bottom surface of the pellicle are rejected.
3. The presence of secondary tracks from other interaction. All the primary beam tracks are followed in backward direction to ensure that the chosen events do not

include interactions from secondary tracks of other interactions. These errors are found to be relatively small so that they do not affect the final result.

## 3.1 Interaction mean free path and cross-section

In the present 3.7A GeV $^{16}$O interaction with emulsion nuclei, a total scanned length of 195.58m primary beam tracks leads to the detection of 1540 events which are attributed to inelastic interactions. In the experimental results, events of elastic scattering of the projectile nuclei are excluded. These events are characterized by one prong emitted with an angle of the secondary track ($\theta \leq 3^{o}$) and having no visible track from the excitation or disintegration of either the incident projectile or the target nucleus. Also the events due to electromagnetic dissociation, i.e. with ($N_h = 0$, $n_s = 0$) are excluded. The events due to elastic interaction and electromagnetic dissociation are 218 events.

As a result, the experimental value of the average mean free path ($\lambda_{exp}$) is found 12.70±0.33 cm, according to the following equation:

$$\lambda_{\exp} = \frac{L}{N} \tag{3-1}$$

where L is the total scanned length and N is the total number of the detected inelastic interactions. The experimental interaction cross section ($\sigma_{exp}$) is 988 ± 25 mb which is determined as:

$$\sigma_{\exp} = \frac{1}{n\lambda_{\exp}} \tag{3-2}$$

where n, is the total atomic density of the nuclear emulsion. It equals to $7.967 \times 10^{22}$ cm$^{-3}$.The inelastic cross section can be calculated theoretically on the basis of the Bradt-Peters formula eq. (1-5).

According to the fitting run by EMU01 and Dubna collaborations [68-70] using projectiles up to $^{56}$Fe and incident energies up to 200A GeV, the Bradt-Peters formula is obtained empirically. First formula is driven by Dubna experiments [68-70] as:

$$\sigma_{cal1} = 10(1.46)^2 \pi (A_P^{(1/3)} + A_T^{(1/3)} - 1.21)^2 \text{ mb} \tag{3-3}$$

The second formula is approximated by EMU01 collaboration [69] as:

$$\sigma_{cal2} = 109.2(A_P^{0.29} + A_T^{0.29} - 1.39)^2 \quad \text{mb} \qquad (3\text{-}4)$$

The total inelastic cross-section can be calculated using the following fomula:

$$\sigma_{inel} = \frac{\sum_i N_i \sigma_i}{\sum_i N_i} \qquad (3\text{-}5)$$

Where Ni is the number of the $i^{th}$ target nuclei per $cm^3$ in the emulsion and $\sigma_{inel}$ is the nucleus-nucleus interaction cross section between the projectile nucleus and $i^{th}$ type of target nucleus. Then the mean free Paths are obtained empirically by substituting the cross-sectional values calculated by equations (3-3) and (3-4) in the following equation:

$$\lambda_{cal} = (\sum_i N_i \ \sigma_i)^{-1} \qquad (3\text{-}6)$$

Table (3-1) shows the experimental values of the average mean free paths for the present $^{16}O$ beam, together with the data for other projectiles P,$^{2}H$,$^{3}He$, $^{4}He$,$^{12}C$,$^{16}O$,$^{22}Ne$,$^{24}Mg$, and $^{32}S$[71-79] interacting in nuclear emulsion at incident energy values of (3.2A - 3.7A GeV). This table also contains the calculated mean free path $\lambda_{cal1}$ and $\lambda_{cal2}$ according to equation (3-3) and (3-4), respectively. According to these results, it may be stated that:

1) The experimental values of the average mean free path decrease with increasing the projectile mass number up to $^{22}Ne$ beyond it which takes a constant value.
2) The empirical predictions of the mean free path values are considerably in agreement with the corresponding experimental ones. This means that the interaction cross-section of the nuclei is successfully explained by the geometrical models with overlapping parameter according to Bradt-Peters equation [26-29].

**Table (3-1):** Experimental values of the average mean free path in the interactions of different projectiles with emulsion nuclei and the corresponding predicted values according to equations (3-3) and (3-4).

| **Projectile** | Energy GeV/A | $\lambda_{exp}$ cm | $\sigma_{exp.}$ mb | $\lambda_{cal1}$ cm | $\lambda_{cal2}$ cm | Ref |
|---|---|---|---|---|---|---|
| **p** | 3.7 | 30.20±0.70 | 391.0±8.0 | 27.82 | 35.15 | 71 |
| **$^{2}$H** | 3.7 | 26.90±0.60 | 495.0±12.0 | 23.60 | 23.74 | 72 |
| **$^{3}$He** | 3.7 | 19.74±0.48 | 622.0±14.0 | 21.21 | 21.22 | 73 |
| **$^{4}$He** | 3.7 | 19.93±0.60 | 629.0±19.0 | 19.43 | 19.47 | 74 |
| **$^{12}$C** | 3.7 | 13.70±0.10 | 871.0±34.0 | 13.36 | 13.49 | 72 |
| **$^{16}$O** | 3.7 | 12.70±0.33 | 988.3±25.0 | 12.12 | 12.31 | This work |
| **$^{16}$O** | 3.7 | 12.18±0.33 | 1039.5±28.2 | 12.12 | 12.31 | 75 |
| **$^{22}$Ne** | 3.2 | 9.92±0.30 | 1265.3±40.0 | 10.49 | 10.71 | 76 |
| **$^{24}$Mg** | 3.7 | 9.60±0.20 | 1115.0±54.0 | 10.12 | 10.35 | 77 |
| **$^{28}$Si** | 3.7 | 9.12±0.27 | 1374.0±37.0 | 9.47 | 9.72 | 78 |
| **$^{32}$S** | 3.7 | 9.55±0.34 | 1359.9±46.2 | 8.94 | 9.20 | 79 |

## 3.2 Projectile fragmentation

A study of projectile fragmentation processes, in general, provides valuable information about the nuclear structure. The projectile fragments PFs essentially travel in the same speed at that of parent beam nucleus, so the energy of the produced PFs is high enough to recognize them easily from the target fragments. All PFs are emitted in a very narrow forward direction cone within an angle $\theta_c \leq 3^o$ given by a Fermi momentum.

### 3.2.1 Charge identification

In the present work, all spectator projectile fragments are recorded and their charges are measured using delta-ray method explained previously in section (2.8.1).

The identification of the charged fragments is made by measuring the total number of δ-ray per mm superimposed on the track. The calibration is done using six primary beams data available in Mohamed El-Nadi high energy laboratory. They are $^{4}$He, $^{12}$C, $^{16}$O, $^{22}$Ne $^{24}$Mg, and $^{32}$S at 3.7A GeV. The relationship between the average number of δ-ray per mm for a sample of 40 tracks from each beam type and the corresponding $Z^2$ is calculated by eq.(2-4).

The calibration data are presented in Fig. (3-1).

The data are fitted by the linear relation:

$$N_{\delta} = AZ^{2} + B \qquad (3\text{-}7)$$

where A and B are the fitting parameters.

$A = 0.171 \pm 0.004$ and $B = -0.420 \pm 0.089$

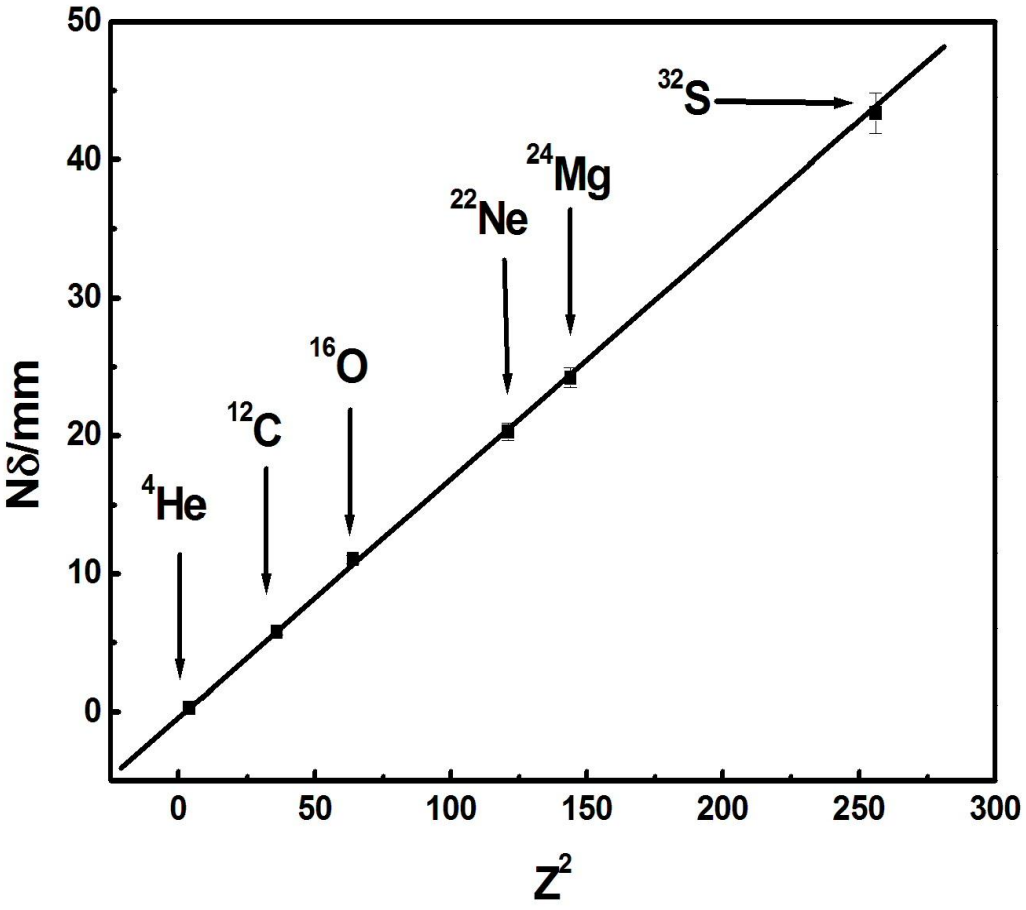


**Fig. (3-1):** Calibration line, showing the relation between the number of δ-ray per mm on the track and $Z^2$ for six primary beams $^{4}He$ , $^{12}C$, $^{16}O$, $^{22}Ne$, $^{24}Mg$, and $^{32}S$ interacting in nuclear emulsion at 3.7A GeV.

The δ-ray frequency distribution (histograms) of projectile fragments having charge Z=3-8 emitted from $^{16}O$ projectile at 3.7A GeV is presented in Fig. (3-2) and can be fitted by Gaussian distribution (smooth curves) with peaks corresponding to certain values of Z. The peak position is a fine indication to the magnitude of the fragment charge. The average value over all the distribution corresponds to the charge and peak position also presented in Fig. (3-3).The data are fitted by the linear relation:

$$\langle N_\delta \rangle = aZ^2 + b \qquad (3\text{-}8)$$

where $a$ and $b$ are the fitting parameters.

$a$ = 0.153±0.006 and $b$ = 0.665±0.283

Unknown charge of possible PFs can be easily identified from δ-ray measurements. The error in $\Delta Z$ = ±0.3 and neglected under $Z \leq 9$ otherwise $\Delta Z$= ±1.

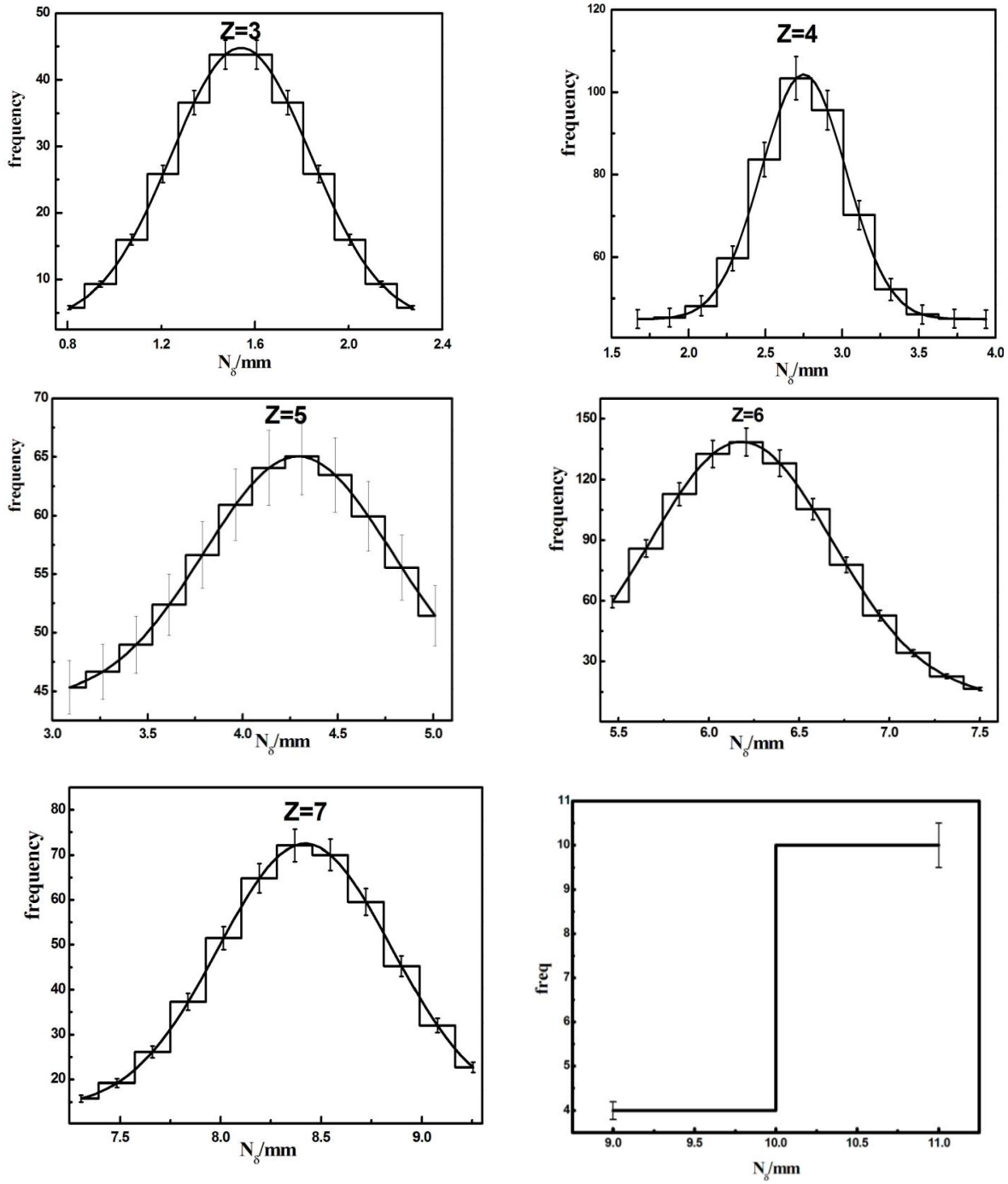


**Fig. (3-2):** δ–ray distributions for secondary projectile fragments due to 3.7A GeV $^{16}$O interactions with emulsion nuclei (histograms) fitted by typical Gaussian shapes (smooth curves).

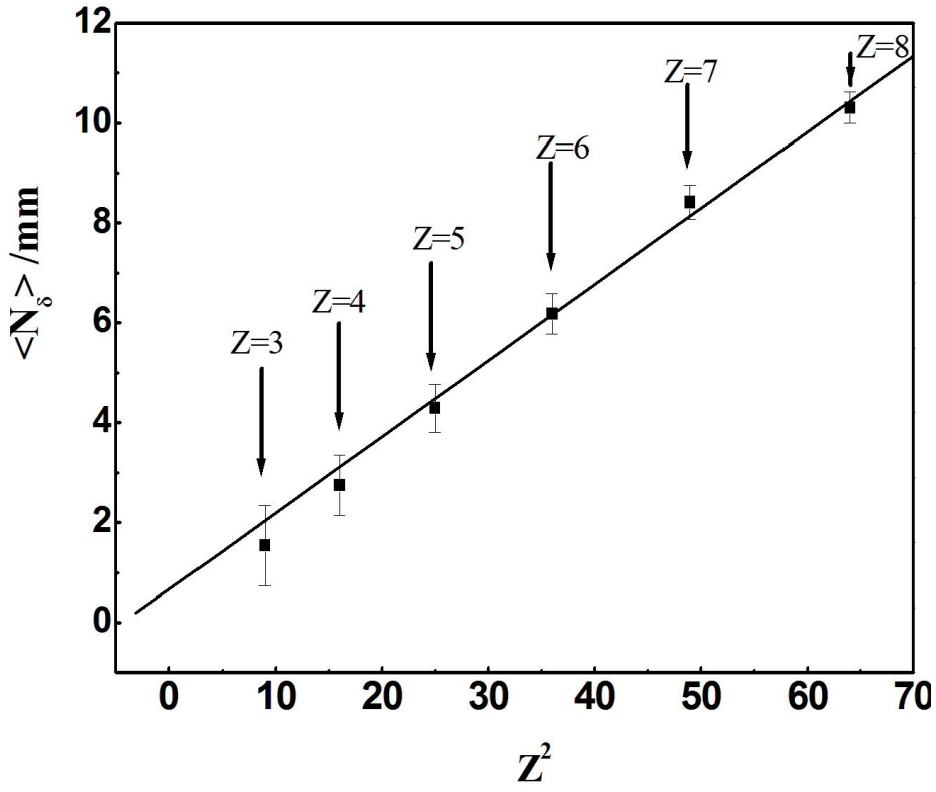


**Fig. (3-3):** Correlation of $\langle N_\delta \rangle$ /mm with $Z^2$ of projectile fragments having Z=3-8 emitted from 3.7A GeV $^{16}$O-Em interactions.

### 3.2.2 Characteristics of the projectile fragments

Table (3-2) gives the topology for all minimum biased events in which each channel includes the participants and the spectators of the oxygen beam obtained from energy 3.7A GeV in comparison with corresponding ones, at energy 60A GeV from our laboratory [80] according to two criteria (Note that in any channel the spectators or PFs have bold symbol but the participants have non bold symbol).

First criteria, according to the nature of charge of fragments. This satisfies that the total charge in each channel should be equal 8.

Second criteria was the classification of the total sample into three groups according to the nature of target nuclei using multiplicity of heavily ionizing secondary charged particle $N_{h.}$ as an experimental parameter for the target size as discussed in section(2.7) . First group with $N_h$=0-1 is interactions with hydrogen. Second group with $N_h$ =2-7 is interactions with light emulsion components CNO. Third group with $N_h \geq 8$ is interactions of $^{16}O$ with heavy emulsion nuclei AgBr.

**Table (3-2):** Topology normalized of the $^{16}$O fragmentation at 3.7 and 60 A GeV [80] (In any channel the spectators or PFs have bold symbol but the participants have non bold symbol).

| $N_h$ | 0-1 | | 2-7 | | ≥8 | | ≥0 | | Fraction of event | Fraction of event |
|---|---|---|---|---|---|---|---|---|---|---|
| Energy A GeV | 3.7 | 60 | 3.7 | 60 | 3.7 | 60 | 3.7 | 60 | 3.7 | 60 |
| Channel | | | | | | | | | | |
| **O** | 0 | 4 | 8 | 0 | 0 | 0 | 8 | 4 | 0.0053 | 0.0042 |
| N + **H** | 10 | 6 | 33 | 7 | 44 | 13 | 87 | 26 | 0.0564 | 0.0275 |
| C + **He** | 4 | 37 | 89 | 60 | 86 | 56 | 179 | 122 | 0.1162 | 0.1292 |
| C + **2H** | 17 | 29 | 86 | 42 | 166 | 49 | 269 | 120 | 0.1746 | 0.1271 |
| B + **He + H** | 1 | 18 | 69 | 19 | 56 | 17 | 126 | 54 | 0.0818 | 0.0572 |
| B + **3H** | 11 | 7 | 26 | 15 | 43 | 15 | 80 | 37 | 0.0519 | 0.0391 |
| Be + **2H**e | 5 | 16 | 85 | 39 | 85 | 40 | 175 | 95 | 0.1136 | 0.1006 |
| Be + **He + 2H** | 0 | 1 | 24 | 7 | 18 | 4 | 42 | 12 | 0.0272 | 0.0127 |
| Be+ **4H** | 1 | 1 | 12 | 3 | 6 | 6 | 19 | 10 | 0.0123 | 0.0105 |
| Li **+ 2He + H** | 1 | 0 | 23 | 1 | 4 | 3 | 28 | 4 | 0.0181 | 0.0042 |
| Li + **He +3 H** | 0 | 1 | 4 | 0 | 2 | 3 | 6 | 4 | 0.0038 | 0.0042 |
| Li+**5H** | 0 | 0 | 0 | 0 | 0 | 0 | 0 | 0 | 0 | 0 |
| He+**Be +2H** | 0 | 0 | 2 | 0 | 0 | 0 | 2 | 0 | 0.0012 | 0 |
| He+ **3He** | 7 | 16 | 70 | 21 | 16 | 15 | 93 | 52 | 0.0603 | 0.0550 |
| He+ **2He + 2H** | 1 | 1 | 8 | 2 | 0 | 1 | 9 | 4 | 0.0058 | 0.0042 |
| He + **C** | 0 | 0 | 15 | 4 | 11 | 4 | 26 | 8 | 0.0168 | 0.0084 |
| H+**3He + H** | 0 | 0 | 5 | 1 | 3 | 0 | 8 | 1 | 0.0051 | 0.0010 |
| H +**2He+3H** | 0 | 0 | 0 | 0 | 0 | 0 | 0 | 0 | 0 | 0 |
| H +**He+ 5H** | 0 | 0 | 0 | 0 | 0 | 0 | 0 | 0 | 0 | 0 |
| Q =0 | 1 | 1 | 123 | 130 | 259 | 229 | 383 | 391 | 0.2487 | 0.4141 |
| All | 59 | 138 | 682 | 351 | 799 | 455 | 1540 | 944 | 1 | 1 |

Figure (3-4) represents the fraction of each channel for all interactions of two oxygen beams at 3.7 and 60A GeV with all emulsion components which are characterized by events with Nh≥ 0. The numbers below represent the magnitude of charges which identified from Z=3 up to 8. The two's numbers which are accompanied some of fragments represent the alpha projectile fragments α-PFs which appear as a special mode of fragmentations for most modes of all possible fragmented nuclei of Z≥ 3. The fraction of each channel of $^{16}$O-nucleus fragmentations is similar at the two projectile energies. It proves that the mechanism which is responsible for projectile fragmentation into all possible channels is independent of the projectile energy but this mode is function only of the essential properties of the parent nucleus of the projectile. Similar conclusion was obtained for other experiment using $^{28}$Si beam interacting with emulsion nuclei at energy 3.7A and14.6A GeV [78].

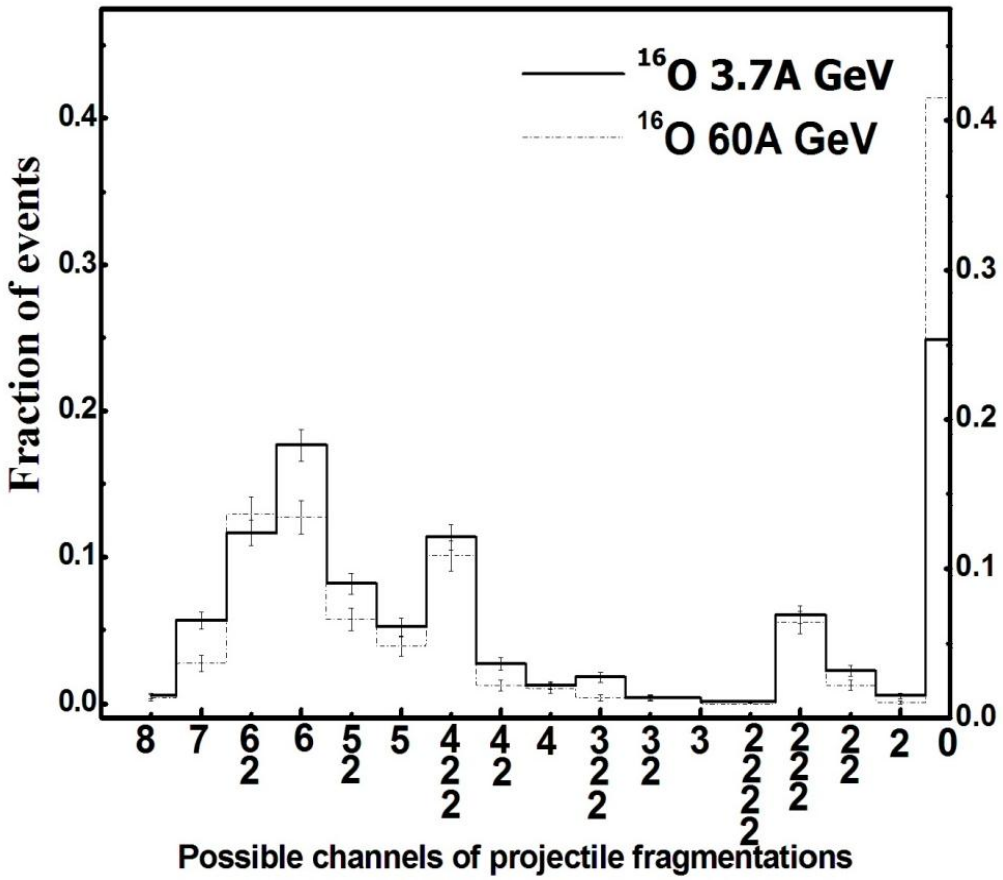


**Fig. (3-4)** Topological diagram for $N_h \geq 0$ events. The numbers below the x-axis represent the charge distribution of the spectators with and without α-fragments.

## 3.3 Experimental evidence of alpha-clusters in $^{16}$O projectile fragmentation process

The study of alpha fragment emission in the projectile fragmentation of $^{16}$O-Em at incident energy 3.7A GeV is presented. The aim is to perform systematic studies on alpha fragment emission in projectile fragmentation. Projectile fragments have considerable advantages, as compared with other experiments on the disintegration of target nuclei. Projectile fragments can be reliably identified and easily distinguished by the emulsion detector used in the present experiment.

Table (3-3), presents the salient features of primary peripheral events of $^{16}$O nuclei at 3.7A GeV in comparison with $^{16}$O nuclei at 60A GeV [80] yielding different α-PF's multiplicities, associated with and without heavy PF's of Z > 2. From the table one can observe that, the data for oxygen strongly reflect the

presence of α-clusters inside the oxygen beam. Moreover the multiplicities of α-particle fragments at the considered energies are nearly similar.

The helium isotopes $^{4}$He and $^{3}$He are emitted in nuclear emulsion by ratios 77.3% and 23.7% respectively.

**Table (3-3):** The normalized multiplicity of α particles, with and without heavy fragments, produced due to the interactions of $^{16}$O at 3.7A and 60A GeV with emulsion nuclei.

| **Energy A GeV** | **1α No. of events (%)** | | **2α No. of events (%)** | | **3α No. of events (%)** |
|---|---|---|---|---|---|
| | **α without heavy fragments** | **α with heavy fragments** | **α without heavy fragments** | **α with heavy fragments** | **α without heavy fragments** |
| **3.7** | **22.9** | **0.8** | **13.76** | **0** | **6.57** |
| **60** | **19.9** | **0.2** | **10.98** | **0** | **5.6** |

### 3.3.1 Dependence of alpha-clusters on incident beam energy

Fig.(3-5) represents the multiplicity distribution of α-PF emitted from inelastic interactions of $^{16}$O with emulsion nuclei at 3.7 A GeV (this work), compared with the corresponding distributions at 2 A GeV [81], 60 A GeV [82] and 200 A GeV [82]. It is shown that the percentage for 1α, 2α and 3α is about 50%, 32% and 15% for the energy of 2A, 3.7A, 60A and 200A GeV $^{16}$O-Em interactions, respectively. This reflects that α-clustering is presented in the structure of oxygen beam and α-multiplicity distribution is independent on beam energy.

It can be explained by considering the process of projectile fragmentation takes a quantization of emissions and takes a form of α-clusters. This quantization mode is independent of incident energy because α-clustering is the initial structure of the parent nucleus before undergoes the processes of fragmentations. Also the possibility of production one α-cluster is easy and more frequent than two α's and gradually decreases because the fragmentation process is non-regular due to the overlapping of projectile with target nucleons which creates a crowded medium of mixed nucleons sufficient for projectile to gradually lose the initial form and regularity of the formation of α-clusters.

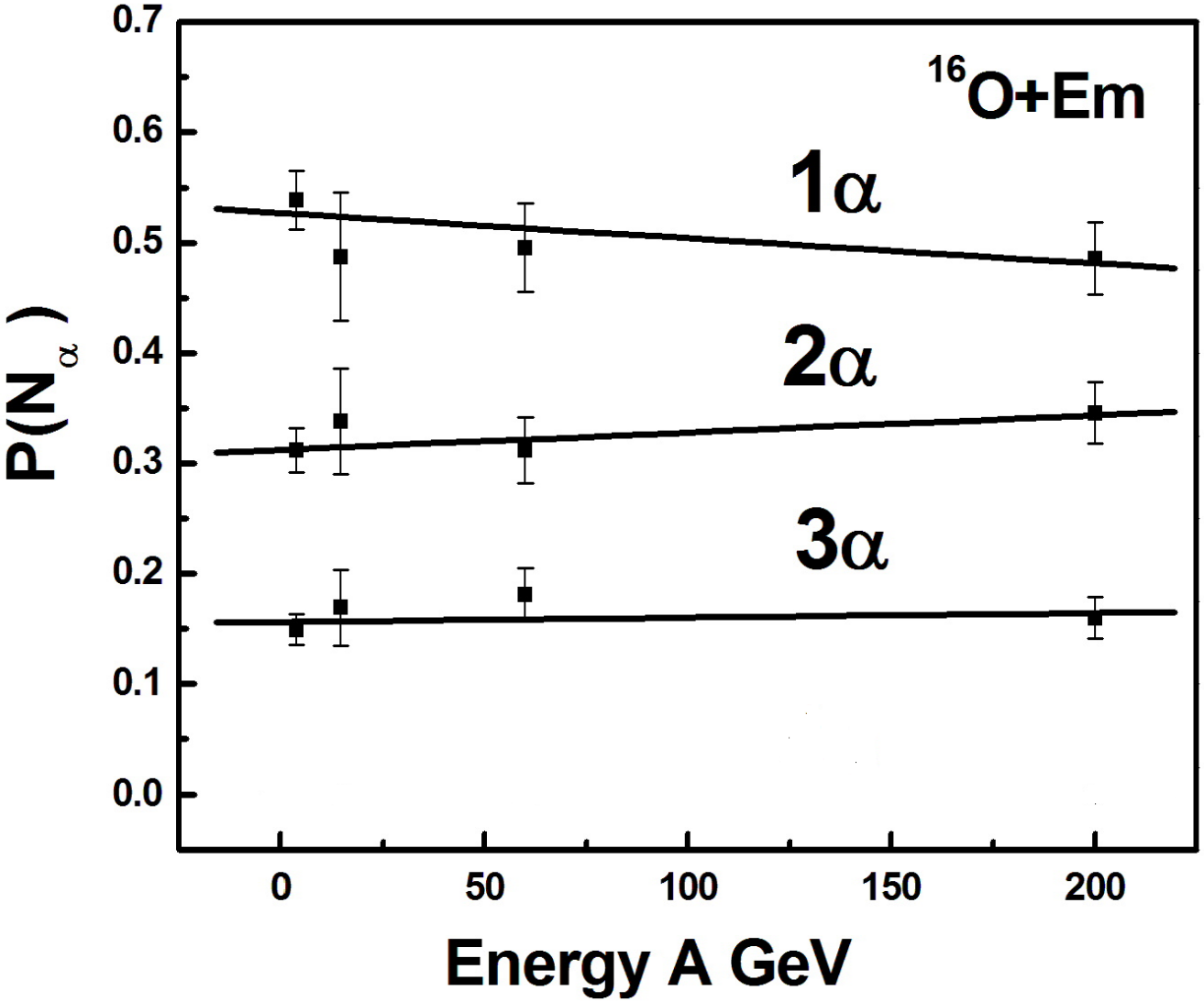


**Fig. (3-5):** The multiplicity distribution of α-projectile fragments emitted from $^{16}$O-Em interactions at the energy of 2A, 3.7A, 60A and 200A GeV.

### 3.3.2 Dependence of alpha-clusters cross-section on the projectile mass number ($A_p$)

The dependence of the inelastic cross-section for collisions with production of α-PF on the projectile mass number is shown in fig (3-6) [83, 84]. The figure shows that the cross-section of emission of single and double alpha fragment strongly depends on the projectile mass number and this dependence gradually disappears with 3α production, i.e. the formation of α-cluster higher than one, shows a negative effect on projectile nucleus to save its initial structure of α-clusters.

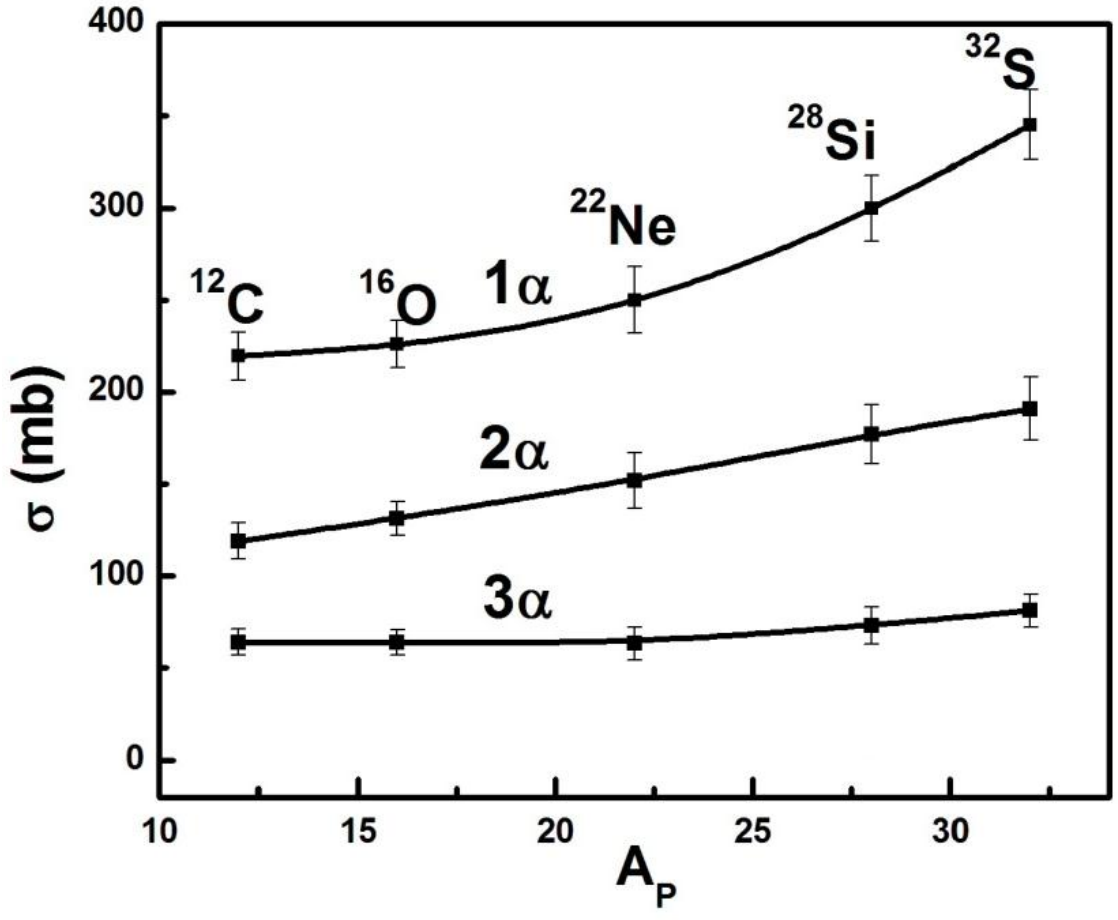


**Fig. (3-6):** The dependence of inelastic cross-section for collisions responsible for production α-cluster on projectile mass number. Solid lines represent the corresponding changes.

### 3.3.3 Dependence of alpha-clusters on the target size

Another interesting point in this investigation is the dependence of multiplicity of α-PF on the target size. In this experiment, the target is composite detector. It can be in general classified into three major classes which are of (Ag, Br) having averaged $A_T$ =94 for heavy, (C, N, O) nuclei having averaged $A_T$ =14 for light and the free hydrogen nucleus having $A_T$ =1. Experimentally, the classification of these interactions is characterized by multiplicity of heavily ionizing secondary charged particle $N_h$. Interactions with light emulsion components CNO are identified with $2 \leq N_h \leq 7$ (gentle interaction) while the interactions with AgBr (hard interaction) is characterized by $N_h \geq 8$. Interactions with hydrogen characterized with $N_h \leq 1$ are excluded due to low statistics. Fig. (3-7) shows the frequency distributions of α-PF for interactions of $^{16}O$ with CNO and AgBr nuclei at collision energy 3.7 A GeV versus multiplicity of $N_h$. For each kind of target the distribution probability of α-PF remains constant at a value in specific range of $N_h$ and gradually decreases with the emission of more than of one α-PF. This behavior is noticed for both gentle and hard interactions. It is normal behavior for the production of projectile fragmentations in both interactions regardless of their target size. For each multiplicity of α-PF, the distribution probability for hard interactions is lower than the corresponding channel for gentle interactions. This will be understood if considering the negative effect of target size on structure of projectile nucleus to save its initial form of α-clusters. It could be explained that the nucleons condense into alpha-particles when the density falls to about one-third of the central nuclear density. This suggests that alpha–particle formation may be energetically favoured in the region of the nuclear surface. In the nuclear interior it is less favoured, but this does not prevent the transient formation of alpha clusters in that region [85]. This means that the experimental observation supports the theory of cluster, which based on the presence of clusters in the parent nucleus before it penetrates

the nuclear barriers and reaches the session configuration after running down the Coulomb barrier.

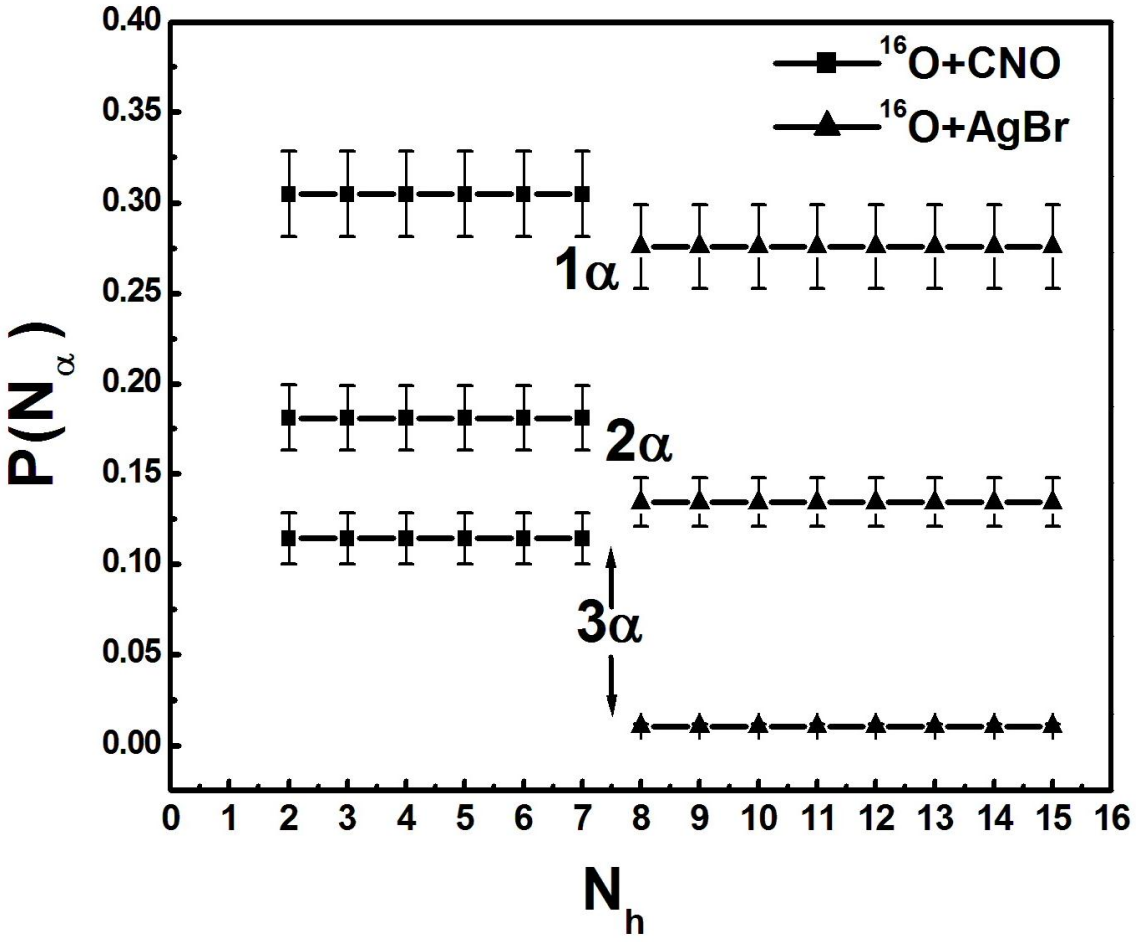


**Fig.(3-7):** Probability distribution of α-cluster multiplicity with interaction of two emulsion components CNO and AgBr versus multiplicity of secondary heavily ionizing charged particles $N_h$.

### 3.3.4 Dependence of alpha-clusters on the projectile size

Another point of interest is the dependence of average multiplicity of $\langle N_\alpha \rangle$ on the projectile mass number. Such dependence is shown in fig (3-8) [83, 84]. This dependence is usually parameterized data in the following power law form in eq. (3-9). It can be explained by considering the increasing in projectile participant nucleons which causes high average number of multiplicity of α-PF.

$$\langle N_\alpha \rangle = a_i A_p^{bi} \qquad (3\text{-}9)$$

$a_i = 0.167 \pm 0.005$
$bi = 0.552 \pm 0.003$

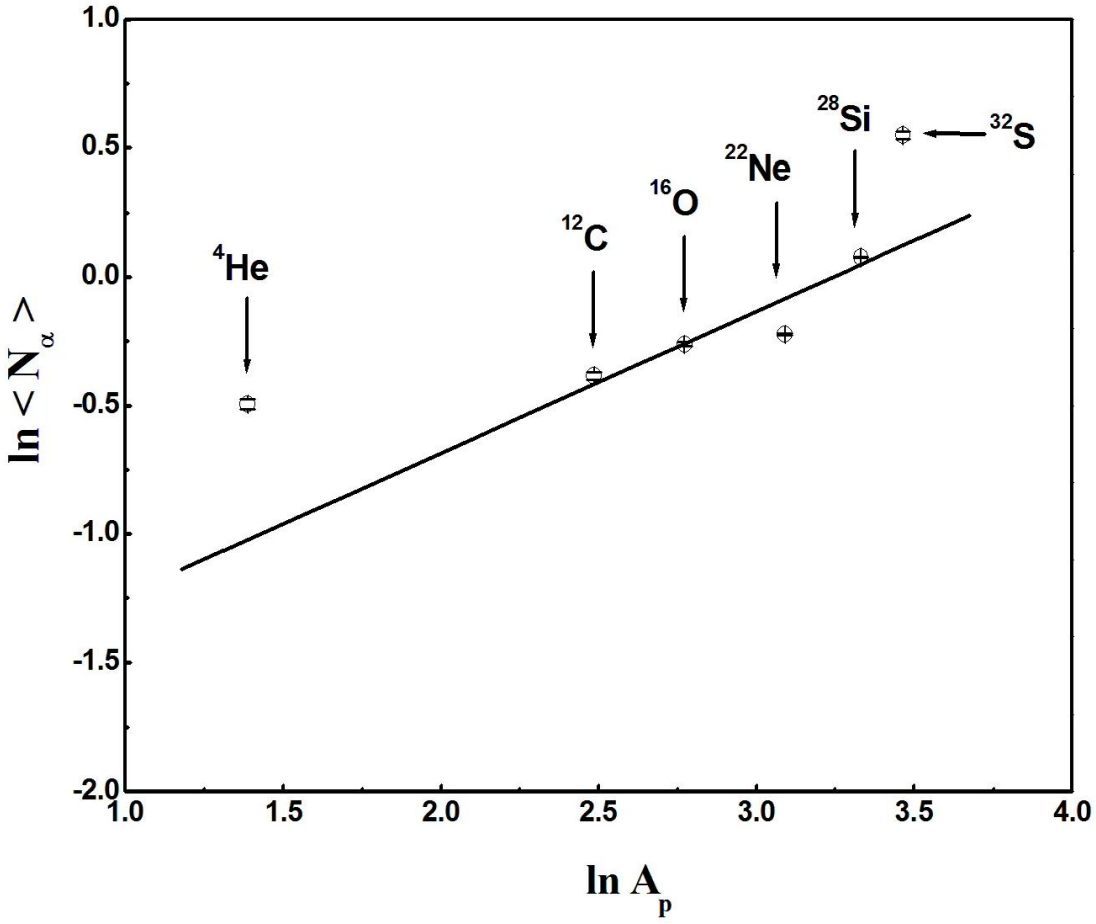


**Fig. (3-8):** The variation of the average multiplicity of α-projectile fragments as a function of the projectile mass number $A_p$. The solid line represents a theoretical fitting of the data given by Eq. (3-9).

### 3.4 Charge multiplicity distribution for all possible fragments

Other point of interest is investigating the special behavior of $^{16}$O projectile fragmentation to produce α-PF than other possible fragments. In Fig. (3-9) the charge multiplicity distribution of all projectile fragments emitted in interactions of $^{16}$O with emulsion at energy 3.7 A GeV is displayed. As a comparison the fragments emitted in $^{16}$O-Em at 60A GeV [80] is also presented. It is noticed that the most abundant PF is that with Z=2 (α cluster) and the next one is for Z=6 (C).The least abundant charges are for Z=3 (Li fragment), Z=5 (B fragment) and Z=7(N fragment). This may be attributed to the fact that for C is considered as combinations of three of α-PF but for B, N and Li that have odd number of protons and far from the α-cluster formations. This concludes that $^{16}$O nucleus is series of cohesive of α-clusters, i.e. α-cluster may be the building block of nuclei. Similar results are obtained for the fragmentation of $^{16}$O-Em at 60 A GeV, i.e. the production mechanism of projectile fragmentations doesn't show any dependence on the projectile energy for all fragment channels.

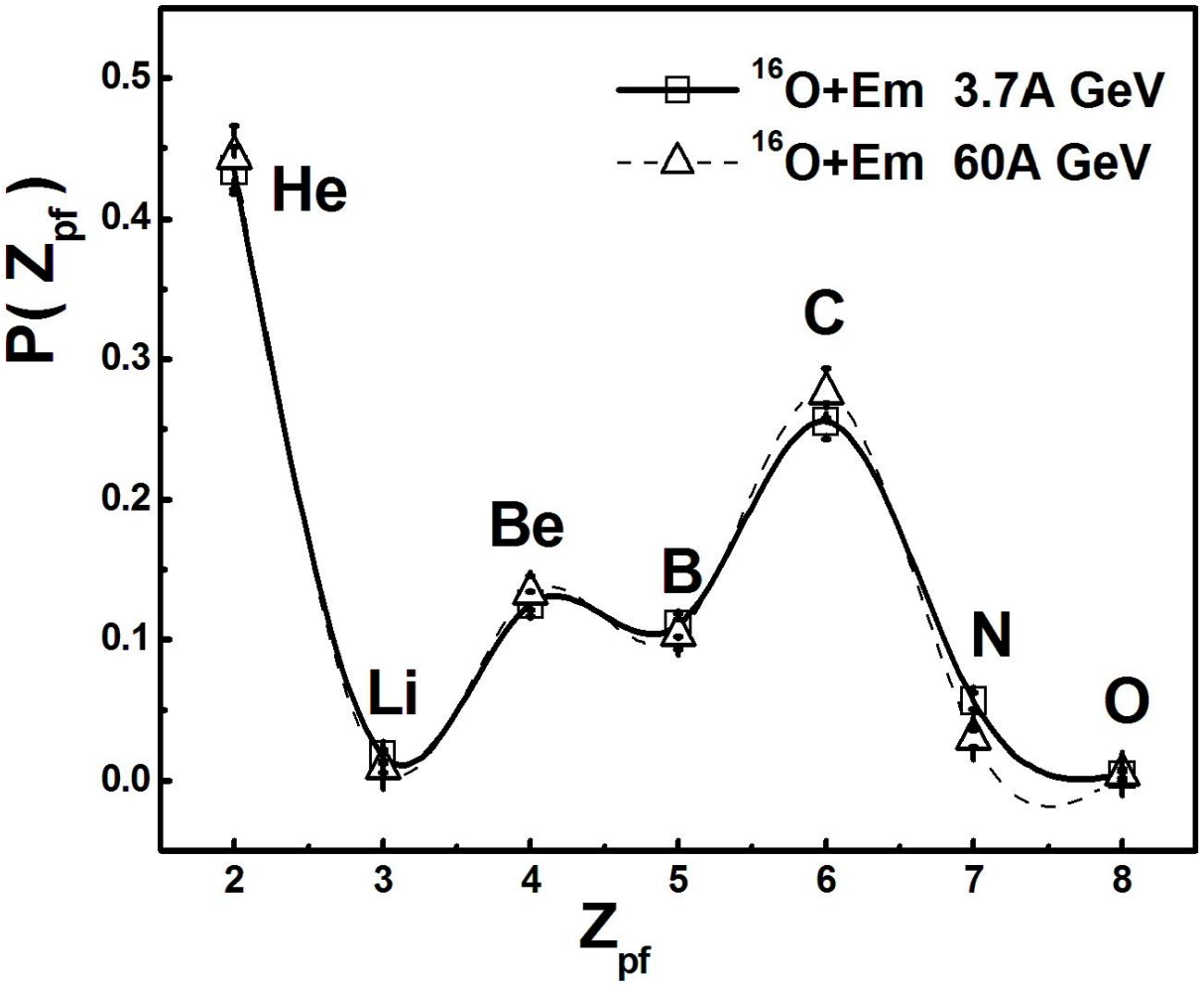


**Fig.(3-9):** Charge multiplicity distribution for of all possible fragments emitted from $^{16}$O-Em at 3.7A and 60 A GeV.

### 3.5 Projectile fragments with Q ≥ 1

Figs.(3-10) shows the probability distribution for emitting fragments with given values of Q where Q =$\sum Z_{PFs}$, i.e. it measures the total charge of all projectile fragments emitting within the fragmentation cone. The value of Q characterizes by the volume of nonoverlapping part of the projectile nucleus. Data at 60A GeV$^{16}$O-Em [80] is also represented. In general both curves show that the behavior of fragmentation process is independent of the incident projectile energy.

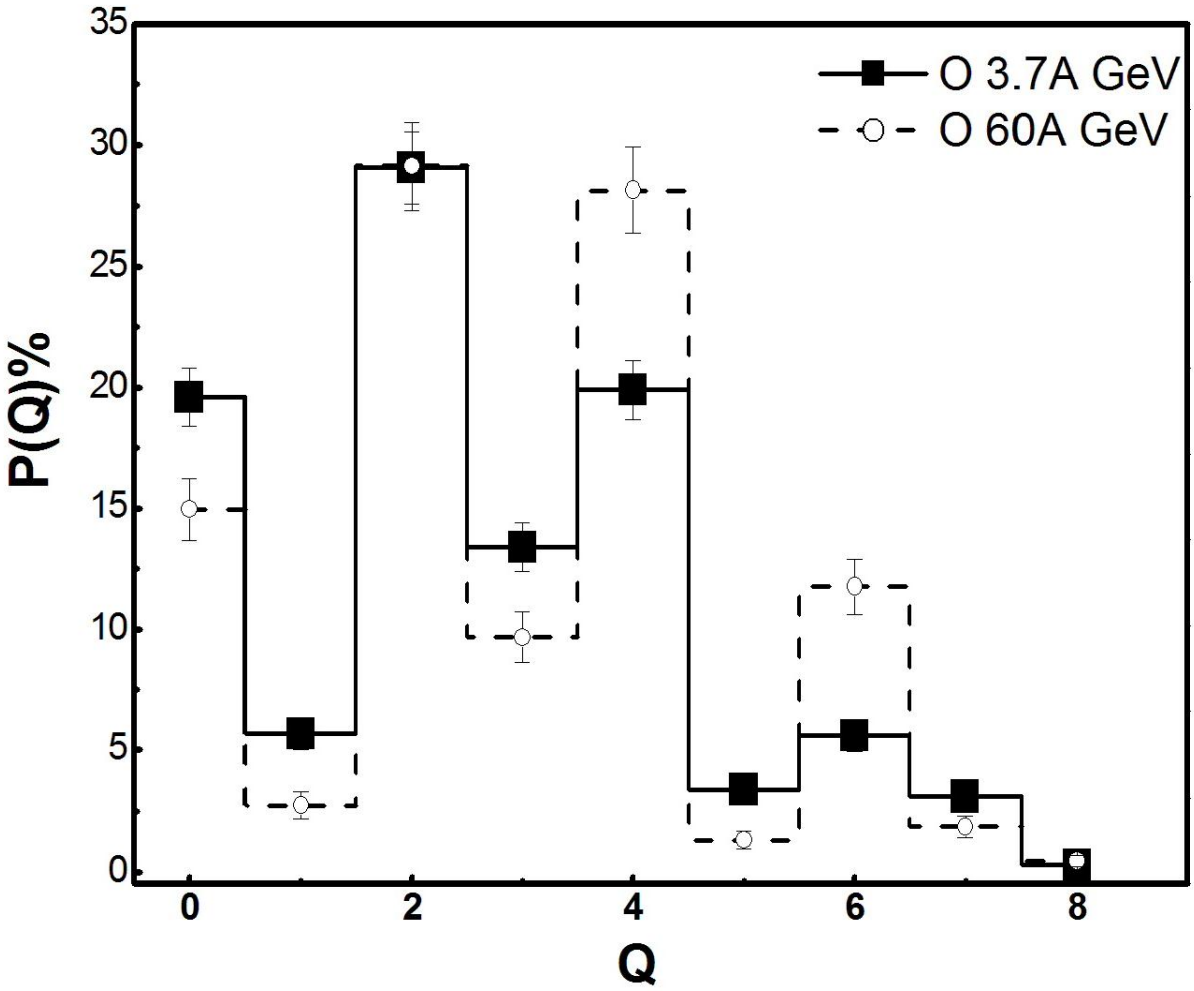


**Fig. (3-10):** The distribution of events with a given value of Q for $^{16}$O-Em at 3.7A and 60A GeV.

## 3.6 Analysis of neutron n and singly charged particle Z=1 multiplicities induced by collision of 3.7A GeV $^{16}$O with target emulsion

In this section two samples of a special type of events have been chosen. 61 events having eight stripped charged particles of the incident are chosen, i.e. $\sum Z_{PF}$ =8. In these events one neutron will collide.

87 events having seven stripped charged particles of the incident are also selected, i.e. $\sum Z_{PF}$ =7. In these events one singly charged particle Z=1 will collide.

### 3.6.1 Topology normalized for n and Z=1from $^{16}$O fragmentation at 3.7A GeV with emulsion nuclei

Table (3-4) shows the distribution of all channels of events emanating from $^{16}$O fragmentation for the two present samples $\sum Z_{PF}$=8 and $\sum Z_{PF}$ =7 corresponding to interactions of n and Z=1 respectively.

It is noticed that when n collides, 49% of its collisions include projectile spectator with oxygen isotopes $_8O^{15}$, 20% associated with 2PFs, one of them has single charge 8% or double charge 12% and 31% associated with more than 2PFs.

On the other hand, for Z=1 the channel of high probability 37% having one projectile spectator with nitrogen $_7N^{14}$, 34% associated with 2PFs, one of them has single charge 22% or double charge 12%, and 29% associated with more than 2PFs.

Concerning the α-PFs production in n and Z=1 events, one can find that 38% and 41% of events respectively having at least one α-PF. This strongly supports the presence of α-clusters inside the oxygen nucleus.

**Table (3-4):** Topology of 3.7A GeV $^{16}O$ events having $\sum Z_{PF}=8$ and $\sum Z_{PF}=7$ in emulsion nuclei.

| **Channels observed $\sum Z_{PF}=8$** | **Number of events (percentage) due to neutron n interaction** | **Channels observed $\sum Z_{PF}=7$** | **Number of events (percentage) due to Z=1 interaction** |
|---|---|---|---|
| $_8O^{16}\rightarrow_8O$ | 30 (49%) | $_8O^{16}\rightarrow_7N$ | 32 (37%) |
| $_8O^{16}\rightarrow_7N+H$ | 5 (8%) | $_8O^{16}\rightarrow_6C+H$ | 19 (22%) |
| $_8O^{16}\rightarrow_6C+_2He$ | 7 (12%) | $_8O^{16}\rightarrow_5B+_2He$ | 10 (12%) |
| $_8O^{16}\rightarrow3_2He+2H$ | 6 (10%) | $_8O^{16}\rightarrow3_2He+H$ | 15 (17%) |
| $_8O^{16}\rightarrow_5B+_2He+H$ | 4 (6.5%) | $_8O^{16}\rightarrow_4Be+_2He+H$ | 5 (5.5%) |
| $_8O^{16}\rightarrow4\ _2He$ | 2 (3.2%) | $_8O^{16}\rightarrow_3Li+2_2He$ | 1 (1%) |
| $_8O^{16}\rightarrow_5B+3\ H$ | 1 (1.6%) | $_8O^{16}\rightarrow2_2He+3H$ | 5 (5.5%) |
| $_8O^{16}\rightarrow_6C+2\ H$ | 2 (3.2 %) | - | - |
| $_8O^{16}\rightarrow_4Be+2\ _2He$ | 4 (6.5%) | - | - |
| All | 61 | All | 87 |

### 3.6.2 Multiplicity distribution of secondary charged particles produced from neutron n and single charged particle Z=1

Fig. (3-11) represents the experimental normalized multiplicity distribution of shower particles $N_s$ for the two selected types according to the participation of Z=1(heavy solid histogram) and n (dashed histogram) from $^{16}O$ with emulsion nuclei at 3.7A GeV. P-Em data at 3.7A GeV is also displayed [86]. The data are systematically compared with predictions of cascade-evaporation model (CEM) [51, 87].All distributions follow the same trend and the CEM model is quite satisfactorily for the three distributions.

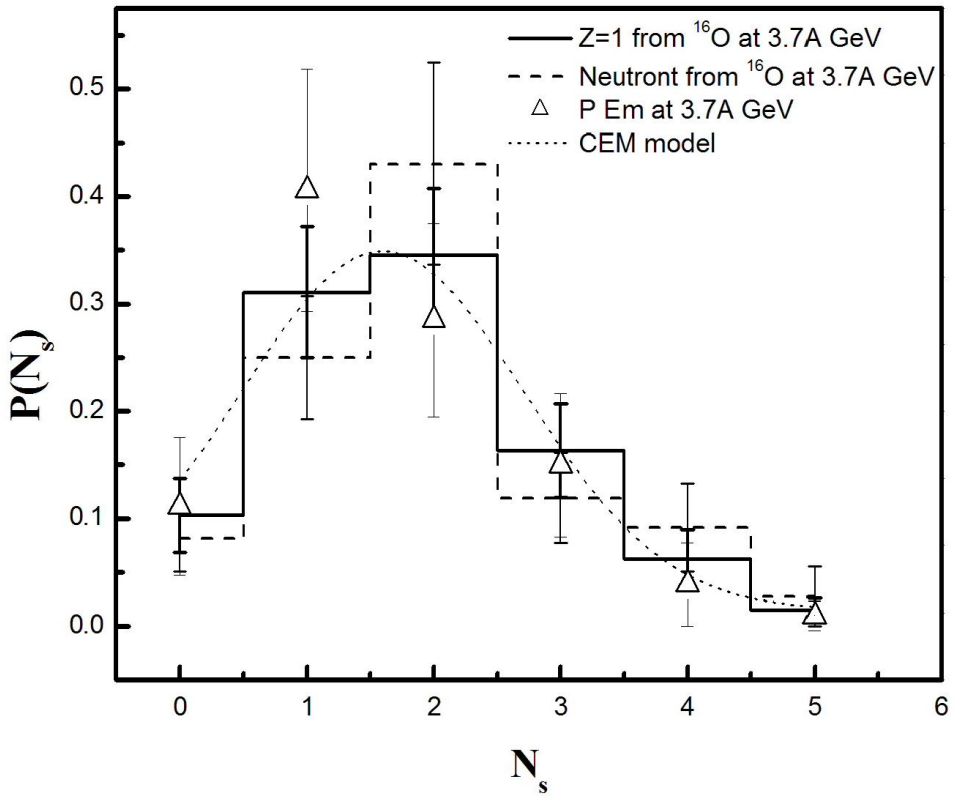


**Fig. (3-11):** Normalized multiplicity distribution of shower particles $N_s$ produced in the participation of Z=1(heavy solid histogram) and n (dashed histogram) from 3.7A GeV $^{16}O$with emulsion nuclei. The triangle is P-Em data. The dot curve represents the CEM predictions.

### 3.6.3 Multiplicity distribution of grey and black particles produced of neutron n and Z=1

Figs. (3-12) and (3-13) represent the experimental normalized multiplicity distribution of grey particles $N_g$ and black particles $N_b$ for the two selected types according to the participation of n (dashed histogram) and Z=1(heavy solid histogram) from $^{16}O$ with emulsion nuclei at 3.7A GeV as well as p-Em data is represented [86]. Similarly as done in Fig. (3-11) the data are systematically compared with predictions of cascade-evaporation model (CEM) [51, 87]. From these two figures one can conclude the following observations:

1- All distributions follow the same trend but the $N_g$ and $N_b$ distribution for p-Em shows different trend and has a long tail up to $N_g$=12 in Fig.(3-12) and up to $N_b$=16 in Fig.(3-13).

2- The CEM model cannot quite successfully describe the general trend of grey and black particles of n and Z=1, while the model describes satisfactorily Ng and $N_b$ distribution of p-Em and predicts its average value.

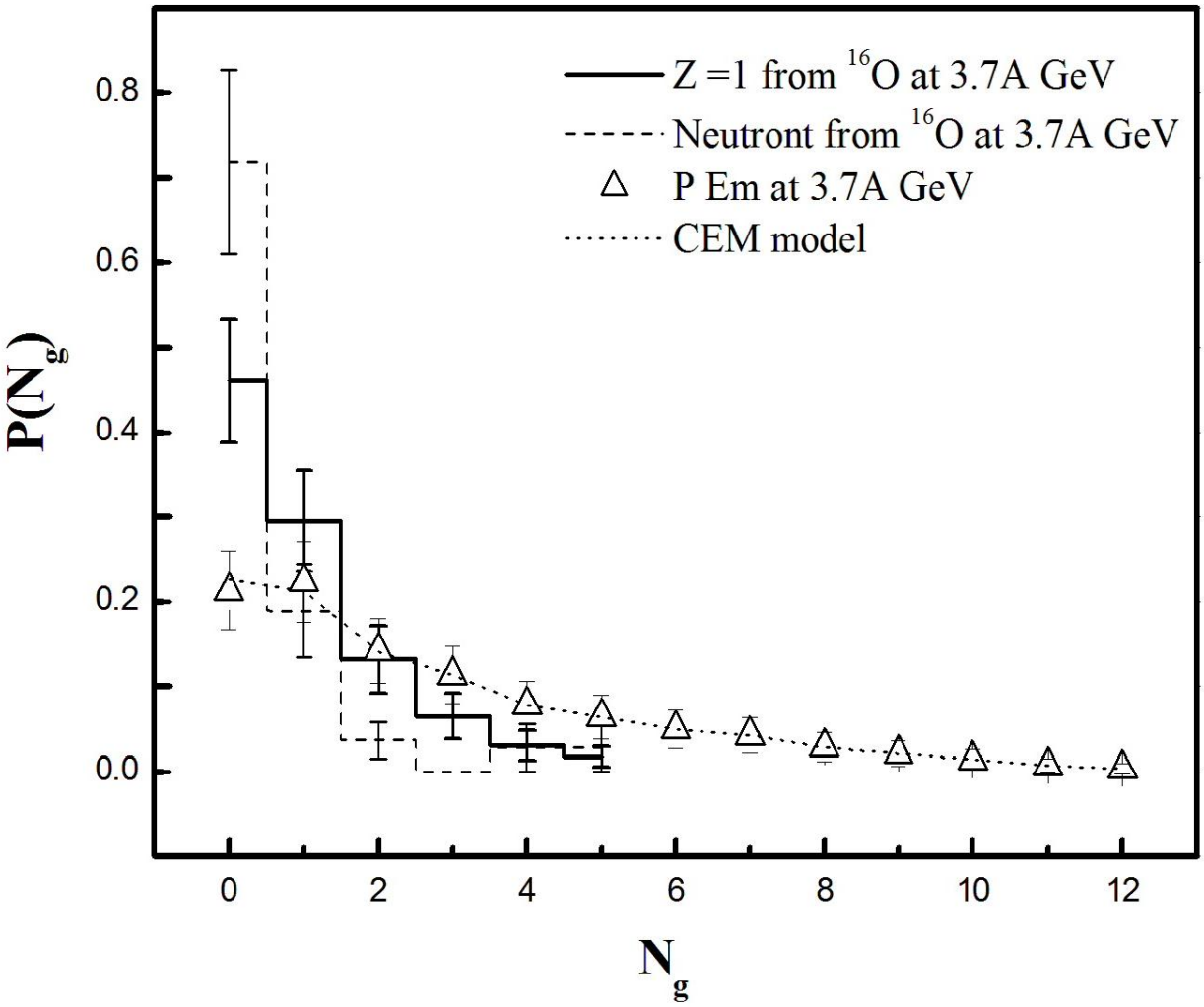


**Fig. (3-12):** Normalized multiplicity distribution of grey particles $N_g$ produced in the participation of Z=1(heavy solid histogram) and n (dashed histogram) from 3.7A GeV $^{16}O$ with emulsion nuclei. The triangle is P-Em data. The dot curve represents the CEM predictions.

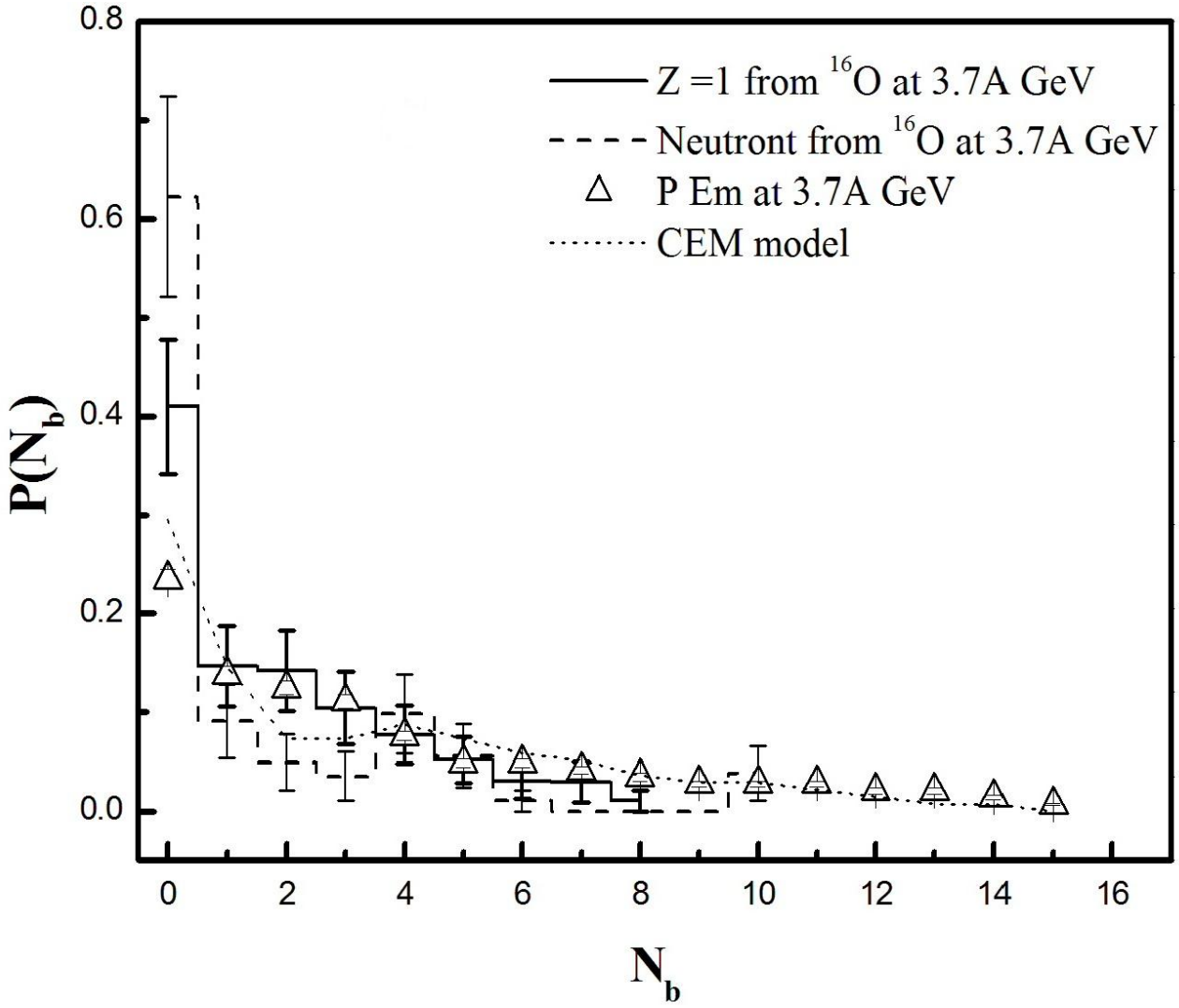


**Fig. (3-13):** Normalized multiplicity distribution of black particles $N_b$ produced in the participation of Z=1(heavy solid histogram) and n (dashed histogram) from 3.7A GeV $^{16}O$ with emulsion nuclei. The triangle is P-Em data. The dot curve represents the CEM predictions.

Table (3-5) displays the average values $\langle N_s \rangle$, $\langle N_g \rangle$ and $\langle N_b \rangle$ produced from n and Z=1 participated in $^{16}O$ interaction with emulsion. p-Em data and CEM predictions are also included.

A small increase in $\langle N_s \rangle$ for Z=1 from $^{16}O$ could be due to the interacting part of Z=1 which may be occurred through few hydrogen isotopes (p, $_1H^2$ and $_1H^3$ and their production ratios in nuclear emulsion are 77.6%, 19.1% and 3.3% respectively[88]). The Z=1 events are thus a contamination of hydrogen isotopes.

**Table (3-5):** Average values of shower $N_s$, grey $N_g$ and black $N_b$ produced from nucleon n and Z=1 participated in $^{16}O$ interaction with emulsion in comparison with p-Em collision and CEM predictions.

| | Present work | | P-Em Ref. [86] | | CEM Ref. [51, 87] | |
|---|---|---|---|---|---|---|
| | Neutron n | Z=1 | (All events) | $N_h \leq 6$ | (All events) | $N_h \leq 6$ |
| $\langle N_s \rangle$ | 1.47±0.18 | 1.86±0.21 | 1.63±0.02 | 1.68±0.03 | 1.75 | 1.8 |
| $\langle N_g \rangle$ | 0.54±0.06 | 0.75±0.08 | 2.81±0.06 | 1.21±0.03 | 2.71 | 1.14 |
| $\langle N_b \rangle$ | 1.35±0.17 | 1.83±0.21 | 3.77±0.08 | 1.39±0.04 | 3.29 | 1.0 |

Figs. (3-12) and (3-13) with table (3-5) show that there is a strong discrepancy between the present data in one side and the equivalent data for p-Em in addition the predictions of CEM in the other side.

This disagreement can be interpreted if one assumes that for the two chosen classes of events (n and Z=1 participating in $^{16}$O-Em interactions) the stripped nucleons interact only with one free or quasi free nucleon with the absence of cascading in other words to make N-N collisions.

In order to support this explanation Fig. (3-14) and Fig. (3-15) show the multiplicity distribution of grey and black particles for events having $N_h \leq 6$. These events theoretically have at least one collision with the stripped n and Z=1.

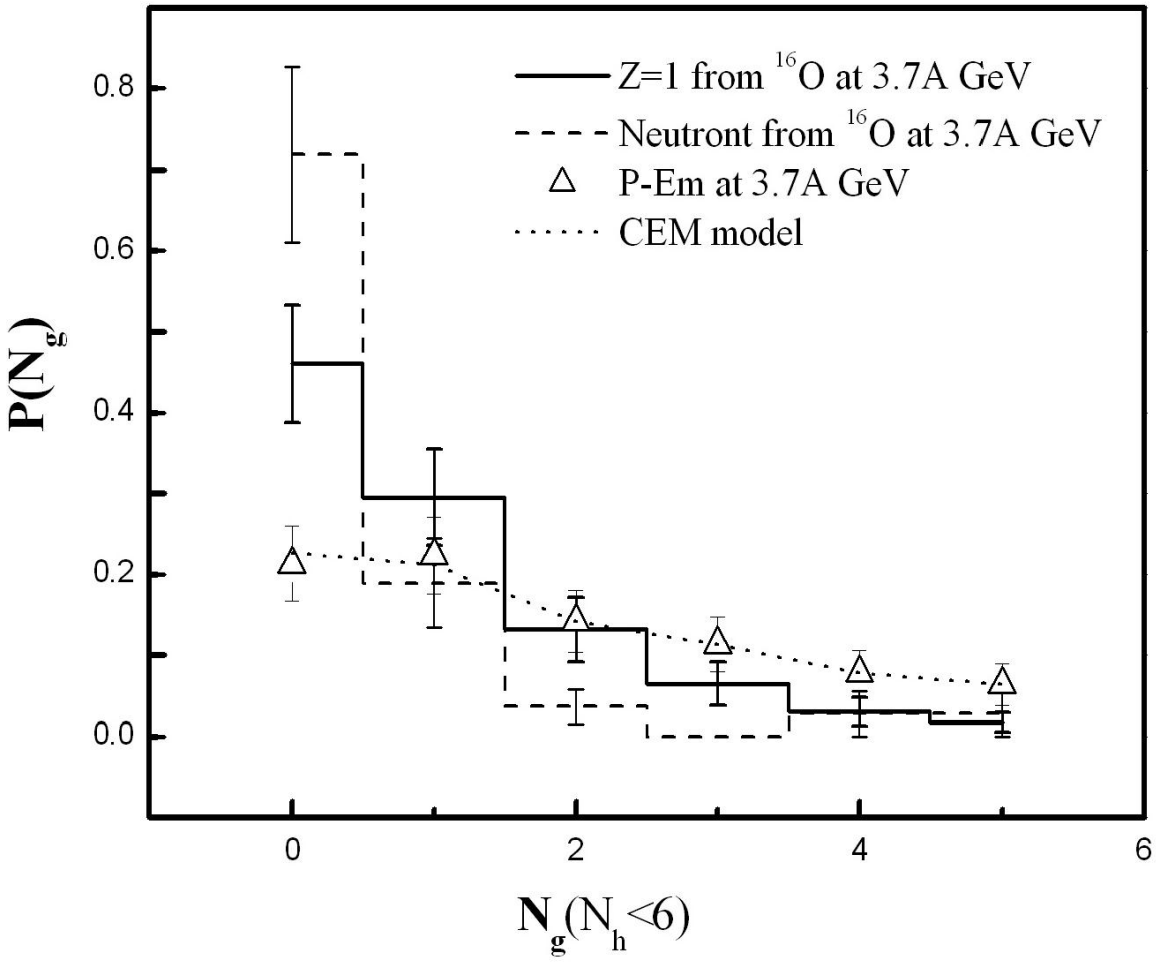


**Fig. (3-14):** Normalized multiplicity distribution of grey particles $N_g$ in events with $N_h \leq 6$ produced in the participation of Z=1(heavy solid histogram) and n (dashed histogram) from 3.7A GeV $^{16}$O with emulsion nuclei. The triangle is p-Em data. The dot curve represents the CEM predictions.

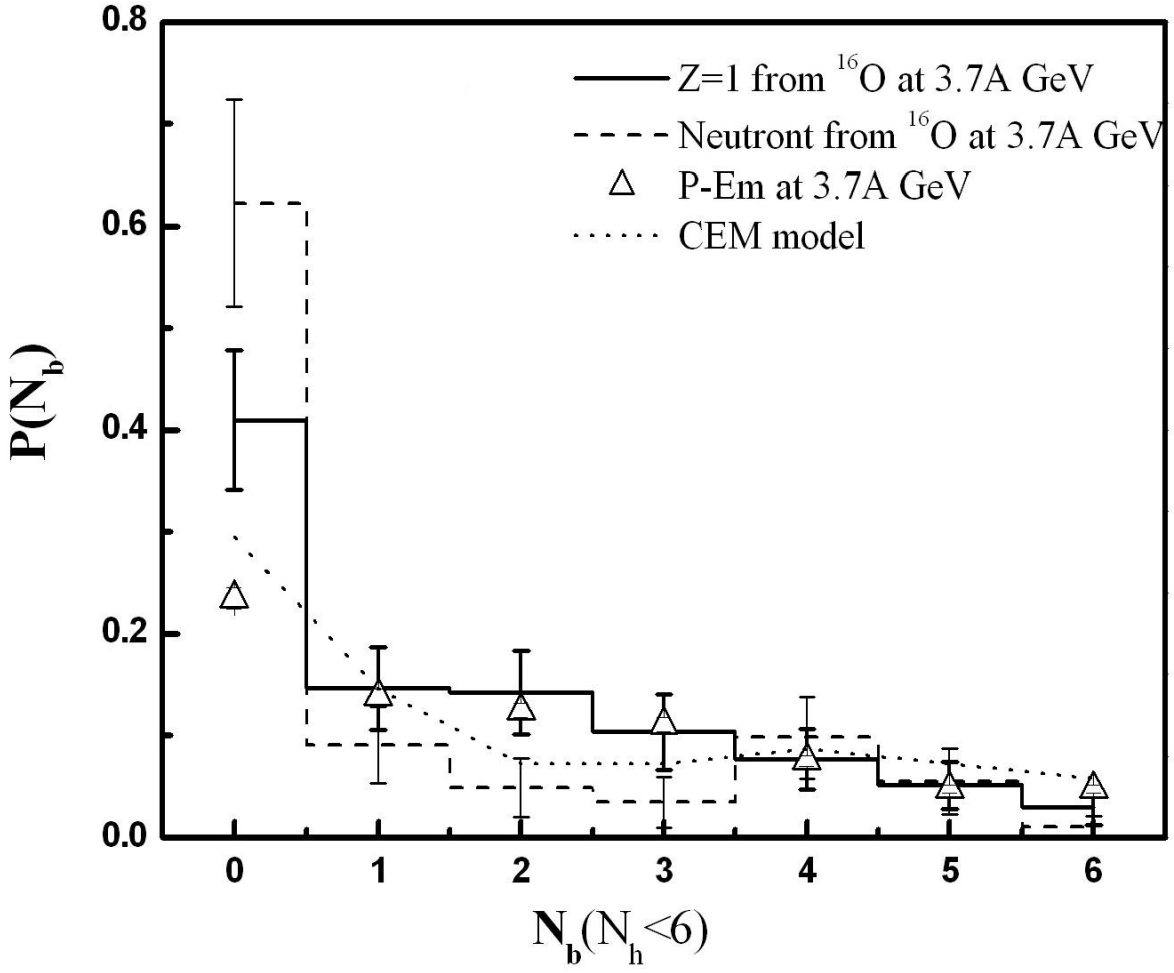


**Fig. (3-15):** Normalized multiplicity distribution of black particles $N_b$ in events with $N_h \leq 6$ produced in the participation of Z=1(heavy solid histogram) and n (dashed histogram) from 3.7A GeV $^{16}O$ with emulsion nuclei. The triangle is p-Em data. The dot curve represents the CEM predictions.

# ***Conclusion***

From studying the inelastic interactions of $^{16}$O ions with emulsion nuclei at incident energy 3.7A GeV, one can conclude the following:

1. The experimental mean free path $\lambda_{exp}$, for $^{16}$O ions in emulsion is 12.70 ± 0.33 cm. The value of $\lambda_{exp}$ and the corresponding cross section value $\sigma_{inel}$ which equals 988.3±25 mb are close to those obtained in similar experiments. The experimental cross sectional values are in agreement with the empirical expectations of Bradt-Peters formula.

2. The charge of each produced fragment is easily identified using δ-ray measurements with accuracy of unit charge.

3. The topology of projectile fragmentation at 3.7A GeV is nearly the same at 60A GeV. This reflects that the mechanism of projectile fragmentation is independent of the beam energy.

4. The possibility of production of one alpha-cluster is more frequent than two alphas and gradually decreases.

5. α-clustering is presented in the structure of oxygen beam and α-multiplicity distribution is independent of beam energy.

6. The target mass number shows negative effect on the α-clusters production. This is due to the increasing in the number of participant target nucleons which disturb the normal structure of the projectile nucleus to save the initial form of the parent nucleus.

7. The cross-section of emission of single and double alpha fragment strongly depends on the projectile mass number and this dependence gradually disappears with 3α and 4α production i.e. the formation of α-cluster higher than

one, shows a negative effect on projectile nucleus to save its initial structure of α-clusters.

8. The average number of α-cluster multiplicity shows a power law relationship on the projectile mass number.

9. The most abundant PF is that with Z=2 (α cluster) and the next one is for Z=6 (C).The least abundant charges are for Z=3 (Li fragment), Z=5 (B fragment) and Z=7(N fragment). This behavior consider as an experimental evidence for formation of α-clusters as the building block of construction of light nuclei in its normal or ground states.

10. Choosing two classes of events having neutron n and singly charged particle Z=1 participated from $^{16}$O at 3.7A GeV, one can conclude that:

a. 38% and 41% of events respectively having at least one α-cluster as a projectile fragment. This strongly supports the presence of α-clusters inside the oxygen nucleus.

b. The values $\langle N_g \rangle$ and $\langle N_b \rangle$ produced in these two classes are in disagreement with those for p-Em data at the same energy and also with the predictions of CEM model. This may be due to the interactions produced by Z=1 nucleon and neutron occur only with one free or quasi free nucleon with the absence of cascading in other words to make N-N collisions.

# List of publications

1- A. Abdelsalam, M. S. El-Nagdy , A. M. Abdalla and A. Saber, Int. J. Mod. Phys. E 24, 1550084 (2015).

2- A. Abdelsalam, M. S. El-Nagdy, B. M. Badawy, W. Osman, M. M. Mohammad, A. Saber, and M. M. Ahmed, WSP World Scientific Publishing International Conference Proc. of the 6th International Conference on Modern Trends in Phys. Research (MTPR-016), Vol. 9916, (2016) (accepted).

3- M. S. El-Nagdy, A. Abdelsalam, B. M. Badawy, P. I. Zarubin, A. M. Abdalla, M. N. Yasien, A. Saber, M. M. Mohammed and M. M. Ahmed, WSP World Scientific Publishing International Conference Proc. of the 6th International Conference on Modern Trends in Phys. Research (MTPR-016), Vol. 9916, (2016) (accepted).

# ***References***


[1] H. H. Heckman, D. E. Greiner, P. J. Lindstrom, and F. S. Bieser, Science 174, 1130 (1971).

[2] H. A. Grunder, W. D. Hartsough, and E. J. Lofgren, Science 174, 1128 (1971).

[3] A. Darbrowska and B. Wosiek, Acta Phys. B 31, 725 (2000).

[4] J. Hufner and J. Knoll, Nucl. Phys. A 290, 460 (1977).

[5] S. Mallik, G. Chaudhuri and S. Das Gupta, Phys. Rev. C 83, 044612 (2011).

[6] P. I. Zarubin et al., EPJ web conference 66, 11044 (2014).

[7] V. Bradova et al., Few-body systems suppl. 14, 241 (2003).

[8] A. Abdelsalam, M. S. El-Nagdy, A. M. Abdalla and A. Saber, Int. J. Mod. Phys. E 24, 1550084(2015) and references therein.

[9] A. Abdelsalam et al., J. Phys. G: Nucl. Part. Phys. 39, 105104 (2012) and references therein.

[10] CMS Collaboration Phy. Lett. B 695, 424 (2011).

[11] ATLAS Collaboration Phys. Lett. B 694, 327 (2011).

[12] J. C. Hill et al., Phys.Rev.Lett. 60, 999(1988).

[13] J. V. Geaga et al., Phys. Rev. Lett. 45, 1993 (1980).

[14] J.C. Hill et al., Phys. Rev.Lett. 33, 1170 (1974).

[15] D. L. Olsen et al, Phys. Rev. C 24, 1529 (1981).

[16] C. A. Bertulani and G. Baur, Nucl. Phys. A 442, 739 (1985).

[17] C. A. Bertulani and G. Baur, Nucl. Phys. A 458 (1986).

[18] C. Brechtmann and W. Heinrich, Z. Phys. A 331, 463 (1988).

[19] G. Baur and C. A. Bertulani, Phys. Rev. C 34, 1654 (1986).

[20] C. A. Bertulani and G. Baur, Phys. Rev. 163, 299 (1988).

[21] J. Gosset et al., Phys. Rev. C 16, 629 (1977).

[22] R. J. Glauber, "Lectures in Theoretical Physics", (Wiley–Interscience, New York), Vol.I, 315 (1959).

[23] M. K. Hegab, M. T. Hussien and N. M. Hassan, Z. Phys. A 336, 345 (1990) and references therein.

[24] W. Czyz and L. C. Maximon, Ann. Phys. (New York) 52, 59(1969).

[25] A. P. Gasparyan et al., JINR Report 1–12797, Dubna, (1979).

[26] H. L. Bradt and B. Peters, Phys. Rev 77, 54 (1950).

[27] H. L. Bradt and B. Peters, Phys. Rev 80, 943 (1950).

[28] H. L. Bradt and B. Peters, Phys. Rev 74, 1828 (1948).

[29] H. L. Bradt and B. Peters, Phys. Rev 75, 1779 (1949).

[30] A. Goldberg, Nucl. Phys. A 240, 636 (1989).

[31] T. F. Clegharn, P. S. Freier and G. J. Waddington, Can. J. Phys. 46, 572 (1968).

[32] S. Barshay, C. B. Dover and J. P. Vary, Phys. Rev. C 360 (1975).

[33] R. R. Daniel and N. Burgaprusad, IL-Nuovo Cimento 523, 82 (1962).

[34] R. J. Glauber and G. Matiae, Nucl. Phys. B 21, 135 (1970).

[35] R. J. Glauber, In High Energy Physics and Nuclear Structure, Amsterdam, P 315 (1967).

[36] R. J. Glauber, In High Energy Physics and Nuclear Science, North-Holland, Amsterdam, 207,783-799 (1969).

[37] H. H. Heckman et al., Phys. Rev. C 17, 1651 (1978).

[38] D. L. Cheshire et al., Phys. Rev. D 10, 25 (1974).

[39] J. Knoll et al., Nucl. Phys. A 304, 298 (1978).

[40] M. Guylassy et al., Phys. Rev. Lett. 40, 298 (1978).

[41] M. I. Adamovich, et al., Proceedings of the Annual Scientific Conference, Bucharest, Romania, Vol.36, P 85 May (2004).

[42] G. D. Westfall, et al., Phys. Rev. Lett. 37, 1202 (1976).

[43] J. D. Bowman, W. J. Swiatecki, and C. F. Tsang, Lawrence Berkeley Laboratory Report No. LBL-2908 (TID-4500-R61), (1973).

[44] R. Hagedorn, in Cargese Lectures in Physics, edited by E. Schatzmann (Gordon and Breach, New York), VI, P 643 (1973).

[45] A. Z. Mekjian, Nucl. Phys. A 312, 491(1978).

[46] J. I. Kapusta, Phys. Rev. C 16, 1493 (1977).

[47] V. S. Barashenkov et al., Nucl Phys. 14, 522(1959).

[48] V. S. Barashenkov et al., Nucl Phys. 24, 642(1961).

[49] V. S. Barashenkov et al., Nucl Phys. 55, 79 (1964).

[50] V. S. Barashenkov et al., Sov. Phys. Usp 16, 31 (1973).

[51] V. S. Barashenkov and V. D. Toneev, Interactions of High Energy Particles and

Atomic Nuclei with Nuclei, Moskva, Adomizdat, 12 (1972),(in Russian).

[52] A. Ferrari et al., Z. Phys. C 71, 75 (1996).

[53] S. G. Mashnik, Proceedings of a Specialists Meeting Intermediate Energy Nuclear Data: Models and Codes, Paris, 107 (1994).

[54] 11th EMU01- Collaboration Meeting, Dubna, Russia, 193(May 1992).

[55] M. El-Nadi et al., J. Phys. G, Nucl. Part. Phys. 24, 2265 (1998).

[56] Wang Er-Qin et al., Chin. Phys. Lett. 28, 8, 082501 (2011).

[57] M. I. Adamovich et al. (EMU01 Collaboration), Phys. Rev. C 40, 66(1989).

[58] B. Cai-Yan and Z. D. Hai, Chinese J. Phys. C 35, 5, 436 (2011).

[59] M. I. Adamovich et al. (EMU01 Collaboration), Phys. Lett. B 390, 445(1997).

[60] C. R. Meng and D. Hai, Chinese J. Phys. 44, 1 (2006).

[61] S. Fakhraddin and M. Rahim, Phys. Scr. 78, 015101 (2008).

[62] M. El-Nadi et al., J. Phys. G 28, 1251 (2002).

[63] Y. Yuan et al., Int. J. Mod. Phys. E 17, 1319 (2008).

[64] I. Otterlund, Z. Phys. C 38, 65 (1988).

[65] A. Kumar et al., J. Phys. Soc., 81, 124202 (2012).

[66] C. F. Powell, F. H. Fowler, and D. H. Perkins, The Study of Elementary Particles by the Photographic Method, Pergamon Press, 474 (1959).

[67] H. Barkas, Nuclear Research Emulsion, Technique and Theory Academic Press Inc., Vol. I, 49 (1963).

[68] N. Angelov et al., Sov. J. Nucl. Phys. 28, 675 (1978).

[69] E. O. Abdrakhmanov et al., Z. Phys. C 5, 1 (1980).

[70] N. Angelov et al., Sov. J. Nucl. Phys. 33, 4 (1981) and references therein.

[71] B. M. Badawy, Int. J. Mod. Phys. E 18, 643 (2009).

[72] BWDKLMT Collab., Sov. J. Nucl. Phys. 29, 52 (1979).

[73] A. Abdelsalam et al., FIZIKA B 15, 9 (2006).

[74] A. Abdelsalam et al., Journal of Nuclear and Radiation Physics 2, 49 (2007).

[75] M. N. Yasin et al., JETP 84,635 (1997).

[76] B. P. Bannik et al., Sov. J. Nucl. Phys. 52, 982 (1984).

[77] S. El-Sharkawy et al., Phys. Scr. 47, 512 (1993).

[78] M. S. El-Nagdy et al., Journal of Physical Studies 16, 4201 (2012).

[79] M. El-Nadi et al., IL Nuovo Cimento A 111, 1243 (1998).

[80] M. El-Nadi et al., IL Nuovo Cimento A 107, 1 (1994).

[81] B. Judek, Proc. of XIV Int. Conf. on Cosmic Ray, Munich, West Germany(1975), (Max- Plank- Institute Fur. Extra terrestriscke Physik, Carching, West Germany, 2342 (1975).

[82] M.I. Adamovich, et al., Phys. Rev. C 40, No. 1 (1989).

[83] M. El-Nadi, et al., Int. J. of Mod. Phys. E., Vol.2, 381-395 (1993).

[84] G. Singh, A. Z. M. Ismail, and P. L. Jain, Phys. Rev. C 43, 2417 (1991).

[85] P. E. Hodgson, Z. Phys. A349, 197-204 (1994).

[86] M. S. El-Nagdy, S. M. Abdel-Halim and M. N. Yasin, Proceedings of American Institute of physics in 2nd International Conference on Modern Trends in Phys. Research, 0-7354-0233-7/05, P387 (2005).

[87] V. S. Barashenkov et al., Yad. Fiz 13, 743(1971); I. Z. Artykov et al., Acta Phys. B 11, 39(1980).

[88] S. Kamel, W. Osman and M. Fayed, Chinese Physics C Vol.41, 054001(2017).

## الملخص العربي للرسالة

تتناول هذه الرسالة دراسة تشظي وانتاج الجسيمات الناتجة من التفاعلات النووية غير المرنة لأنوية الأكسجينن (16) مع أنوية المستحلب النووي عند طاقة 3,7 جيجا إلكترون فولت لكل نيوكليون ، قد استخدمنا ألواح المستحلبات النووية من النوع NIKFI-BR2 والتي تم تعريضها لأنوية الأكسجين (16) المعجلة بمعامل دوبنا- روسيا.

وعند مسح 195,58 مترا من اثار القذائف تم تحديد ودراسة عدد 1540 من التفاعلات النووية ووجد أن متوسط المسار الحر لهذه التفاعلات هو 12,70±0,33سم ، وهذه القيمة تناظر مساحه مقطع للتفاعل قيمتها 988 ± 25 مللي بارن و وجد أن هذه القيم تقترب من تلك القيم التي تم حسابها من خلال النموذج النظري الذي يعتمد علي الوصف الهندسي للتفاعلات النووية.

لقد تم تحديد الشحنة لجميع الجسيمات الناتجة من تشظي نواة المقذوف بطريقة أشعة دلتا وتصنيفها وتحديد عدد التصادمات المسبب لكل نوع من أنوع هذه الشحنات. كذلك تم دراسة التوزيعات العددية وتوزيعات هذه الشحنات ومقارنتها بمثيلاتها لتفاعل أنوية أكسجين عند طاقة 60 جيجا إلكترون فولت لكل نيوكليون حيث وجد أن هذه التوزيعات لا تعتمد على طاقة المقذوف.

تم دراسة التوزيع العددي لجسيمات ألفا و مقارنتها بمثيلاتها لتفاعل أنوية أكسجين عند طاقة 60جيجا الكترون فولت في محاولة دراسة تكون نواة الأكسجين من حزم ألفا وجد أنه لا يعتمد على طاقة المقذوف. كما تم دراسة اعتمادية تكون نواة الأكسجين من مجموعات من حزم ألفا علي كلا من حجم نواة المقذوف وحجم نواة الهدف.

كما تم دراسة خروج الشظايا الثقيلة لنواة المقذوف ذات الشحنة أكبر من 3 ووجد أنها أيضا لاتعتمد علي الطاقة الساقطة للمقذوف.

كما تم أخذ عينتين من التفاعلات والتي تخص تفاعل النيوترون والجسيم احادي الشحنة المشارك من نواة الأكسجين في التفاعلات وتم تصنيف وتحديد عدد التصادمات المسبب لكل نوع من أنوع هذه التفاعلات.

كما تم عمل التوزيع العددي للجسيمات الثانوية من الهادرونات فائقة السرعة (الجسيمات الرزازية) والهادرونات السريعة ( الرمادية) والبطيئة (السوداء) من هذه التفاعلات وكذلك مقارنتها بمثيلاتها الناتجة من تفاعل البروتون مع أنوية المستحلب النووي عند نفس الطاقة وهي 3,7 جيجاأ الكترون فولت وتم تحليل هذه النتائج ومقارنتها أيضا بنتائج نموذج التبخير المتسلسل (CEM).

وقد أظهرت الدراسة نجاح هذا النموذج في تفسير خروج الجسيمات فائقة السرعة (الجسيمات الرزازية) وفشله في تفسير الجسيمات السريعة (الرمادية) والبطيئة (السوداء).


الله
جل جلاله

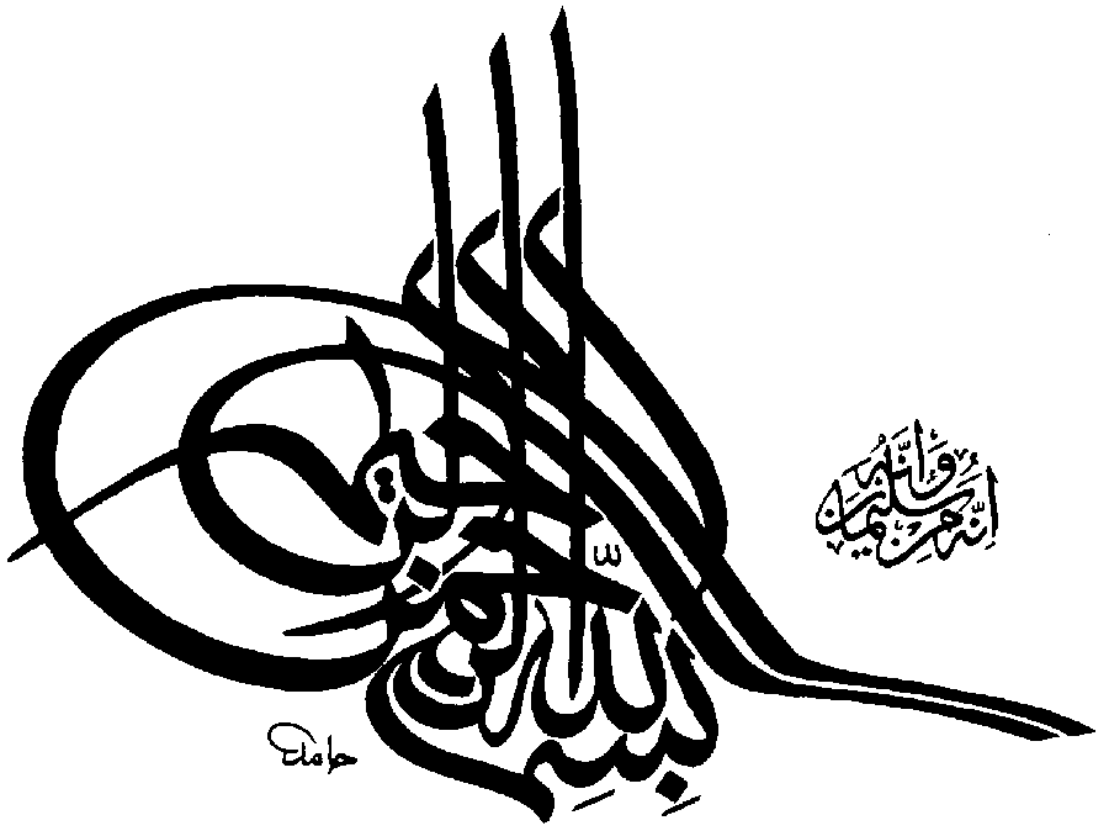
بسم الله الرحمن الرحيم
إنه من سليمان وإنه
حامد

جا معة بنها
كلية الهندسة بشبرا
قسم الرياضيات والفيزيقا الهندسية

# خصائص تشظي أنوية أكسجين ( ١٦ ) المتفاعلة مع أنوية المستحلب النووي عند طاقة ٣,٧ أ جيجا الكترون فولت

رساله مقدمة إلى
جا معة بنها- كلية الهندسة بشبرا
قسم الرياضيات والفيزيقا الهندسية

مقدمة من

**مهندس**

## عبدالناصر صابر عبدالفتاح سليمان

بكالوريوس فى الهندسة الكهربية ( قوى وألات كهربية )
كلية الهندسة بشبرا - جامعة بنها (٢٠٠٥)
ماجستير الفيزياء الهندسية ٢٠١٢
مدرس مساعد بقسم الرياضيات والفيزيقا الهندسية - كلية الهندسة بشبرا- جامعة بنها

للحصول على
**درجة دكتوراة الفلسفة فى الفيزياء الهندسية**

**تحت إشراف**

**أ.د/ عبدالله عبدالسلام محمد**
أستاذ الفيزياء النووية
كلية العلوم- جامعة القاهرة

**أ.د/ بدوي محمد بدوي**
أستاذ الفيزياء النووية - قسم طبيعة المفاعلات - هيئة الطاقة الذرية

**أ.د/ محمد السيد النجدي**
أستاذ الفيزياء النووية
كلية العلوم- جامعة حلوان

**أ.م.د / أحمد محمد عبدالله**
أستاذ الفيزياء الهندسية المساعد
كلية الهندسة بشبرا– جامعة بنها

كلية الهندسة بشبرا - جامعة بنها

٢٠١٧